HHS Public Access

Author manuscript

Nature. Author manuscript; available in PMC 2023 August 07.

Published in final edited form as:

Nature. 2023 April ; 616(7958): 747–754. doi:10.1038/s41586-023-05857-4.

Clonal hematopoiesis and risk of chronic liver disease

Waihay J. Wong[1,3,4,*], **Connor Emdin**[2,4,*], **Alexander G. Bick**[4,5], **Seyedeh M. Zekavat**[4,6,7], **Abhishek Niroula**[1,4,8], **James P. Pirruccello**[2,4,9], **Laura Dichtel**[10,11], **Gabriel Griffin**[4,12], **Md Mesbah Uddin**[4], **Christopher J. Gibson**[1,4], **Veronica Kovalcik**[1], **Amy E. Lin**[1,4,13], **Marie E McConkey**[1], **Amelie Vromman**[13], **Rob S. Sellar**[1,14], **Peter G. Kim**[1,4], **Mridul Agrawal**[1], **Joshua Weinstock**[15], **Michelle T. Long**[16], **Bing Yu**[17,18], **Rajarshi Banerjee**[19], **Rowan C. Nicholls**[19], **Andrea Dennis**[19], **Matt Kelly**[19], **Po-Ru Loh**[4,11,20], **Steve McCarroll**[4,21], **Eric Boerwinkle**[18,22], **Ramachandran S. Vasan**[23,24], **Siddhartha Jaiswal**[25], **Andrew D. Johnson**[26], **Raymond T. Chung**[11,27], **Kathleen Corey**[11,27], **Daniel Levy**[24,28], **Christie Ballantyne**[29,30], **NHLBI TOPMed Hematology Working Group**, **Benjain L. Ebert**[1,4,11,31,#], **Pradeep Natarajan**[2,4,11,#]

[1)]Department of Medical Oncology, Dana-Farber Cancer Institute, Boston, MA 02445, USA

Please address correspondence to: Pradeep Natarajan, MD MMSc, Massachusetts General Hospital, 185 Cambridge Street, CPZN 3.184, Boston, MA 02114, Phone: 617-724-3526, pnatarajan@mgh.harvard.edu, Twitter: @pnatarajanmd. Correspondence and requests for materials should be addressed to P.N. and B.L.E.

*These authors contributed equally to this work.

#These authors co-supervised this work.

The views expressed in this manuscript are those of the authors and do not necessarily represent the views of the National Heart, Lung, and Blood Institute; the National Institutes of Health; or the U.S. Department of Health and Human Services.

Author Contributions

W.J.W., C. Emdin, B.L.E., and P.N. conceived of, designed, and wrote the manuscript for this project. B.L.E. and P.N. provided supervision, project administration, and secured funding. C. Emdin led human genetics data curation and analyses, and W.J.W. led animal experiments and analyses. V.K., A.E.L, M.E.M., A.V., R.S.S., P.G.K., M.A. performed experiments and revised the manuscript for intellectual content. A.B., S.M.Z., A.N., J.P., L.D., G.G., M.U., C.G. contributed to human genetic data and revised the manuscript for intellectual content. R. Banerjee, R.C.N., A.D., M. Kelly analyzed the U.K. Biobank liver imaging data and revised the manuscript for intellectual content. All other authors (J.W., M.T.L., B.Y., P.-R.L., S.M., E.B., V.R., S.J., A.D.J., R.T.C., K.C., D.L., C.B.) revised the manuscript for intellectual content.

Competing interests

W.J.W., C. Emdin, B.L.E. and P.N. are inventors on a US provisional patent application related to this work filed by Massachusetts General Hospital and Dana-Farber Cancer Institute (number 63/116,382, filed 20 November 2020). P.N. reports grant support from Amgen, Apple, AstraZeneca, Boston Scientific and Novartis, and personal fees from Allelica, Apple, AstraZeneca, Blackstone Life Sciences, Foresite Labs, Invitae, Novartis, Roche/Genetech and TenSixteen Bio, is a scientific advisory board member of Esperion Therapeutics, geneXwell and TenSixteen Bio, and reports spousal employment at and equity in Vertex, all distinct from the present work. C. Emdin reports personal fees from Acceleron Pharma, Korro Bio, Navitor Pharma, Nference, Novartis and Third Rock Ventures, all distinct from the present work. B.L.E. has received research financial support from Celgene, Deerfield, Novartis and Calico, and consulting fees from GRAIL, and serves on the scientific advisory boards for Neomorph Therapeutics, Skyhawk Therapeutics and Exo Therapeutics, all distinct from the present work. P.N. and B.L.E. are scientific co-founders of TenSixteen Bio, which focuses on somatic mosaicism and precision medicine. L.D. has received research support from Perspectum Ltd, Pfizer, Lumos Pharma and Recordati, is a MGB Innovation Fellow hosted by Third Rock Ventures (a venture capital firm) and remains full time at MGH during the period of this educational program (anticipated 1 October 2022–30 September 2024); the financial interests of L.D. were reviewed and are managed by MGH and MGB in accordance with their conflict-of-interest policies. M.A. received consulting fees from German Accelerator Life Sciences and is a co-founder of and holds equity in iuvando Health, all unrelated to the present work. R. Banerjee, R.C.N., A.D. and M. Kelly receive salaries from and have stock options in Perspectum and research interests in liver and cardiometabolic disease. S.J. is on advisory boards for Novartis, AVRO Bio and Roche Genentech, is a paid consultant for Foresite Labs, reports speaking fees and an honorarium from GSK, is an equity holder and a scientific advisory board member of Bitterroot Bio, and is a co-founder, equity holder, and scientific advisory board member of TenSixteen Bio. R.T.C. has received grant support to his institution from Abbvie, Boehringer, Gilead, Merck, BMS, Roche, Janssen and GSK all unrelated to the present work. All other authors declare no competing interests.

[2)]Cardiovascular Research Center and Center for Genomic Medicine, Massachusetts General Hospital, Boston, MA 02114, USA

[3)]Department of Pathology, Brigham and Women's Hospital, Boston, MA 02115, USA

[4)]Broad Institute of Massachusetts Institute of Technology and Harvard University, Cambridge, MA 02142, USA

[5)]Division of Genetic Medicine, Department of Medicine, Vanderbilt University Medical Center, Nashville, TN 37232, USA

[6)]Yale University School of Medicine, New Haven, CT 06510, USA

[7)]Department of Ophthalmology, Harvard Medical School, Boston, MA 02114, USA

[8)]Department of Laboratory Medicine, Lund University, Lund, Sweden

[9)]Division of Cardiology, University of California San Francisco, San Francisco, CA 94158, USA

[10)]Neuroendocrine Unit, Department of Medicine, Massachusetts General Hospital, Boston, MA 02114, USA

[11)]Department of Medicine, Harvard Medical School, Boston, MA 02115, USA

[12)]Department of Pathology, Dana-Farber Cancer Institute, Boston, MA 02115, USA

[13)]Division of Cardiovascular Medicine, Department of Medicine, Brigham and Women's Hospital, Boston, MA 02115, USA

[14)]Department of Haematology, UCL Cancer Institute, London, UK

[15)]Department of Biostatistics, Center for Statistical Genetics, University of Michigan School of Public Health, Ann Arbor, MI 48109, USA

[16)]Section of Gastroenterology, Boston Medical Center, Boston University School of Medicine, Boston, MA 02118, USA

[17)]Department of Epidemiology, Human Genetics and Environmental Sciences, School of Public Health, University of Texas Health Science Center at Houston, Houston, TX 77030, USA

[18)]Human Genetics Center, Department of Epidemiology, Human Genetics and Environmental Sciences, School of Public Health, The University of Texas Health Science Center at Houston, Houston, TX 77030, USA

[19)]Perspectum Diagnostics Ltd., Oxford, UK

[20)]Division of Genetics, Department of Medicine, Brigham and Women's Hospital, Boston, MA 02115, USA

[21)]Department of Genetics, Harvard Medical School, Boston, MA 02115, USA

[22)]Human Genome Sequencing Center, Baylor College of Medicine, Houston, TX 77030, USA

[23)]The University of Texas School of Public Health San Antonio, and University of Texas Health Sciences Center, San Antonio, TX 78229.

[24)]Framingham Heart Study of the NHLBI and Boston University School of Medicine, Framingham, MA 01702, USA

[25]Department of Pathology, Stanford University School of Medicine, CA 94305, USA

[26]Population Sciences Branch, National Heart Lung and Blood Institute, Framingham, MA 01702, USA

[27]Liver Center, Division of Gastroenterology, Department of Medicine, Massachusetts General Hospital, Boston, MA 02114, USA

[28]Population Sciences Branch, National Heart, Lung, and Blood Institute, National Institutes of Health, Bethesda, MD 20892, USA

[29]Department of Medicine, Baylor College of Medicine, Houston, TX 77030, USA

[30]Department of Molecular and Human Genetics, Baylor College of Medicine, Houston, TX 77030, USA

[31]Howard Hughes Medical Institute, Dana-Farber Cancer Institute, Boston, MA 02215, USA

Summary

Chronic liver disease is a major public health burden worldwide[1]. Although different aetiologies and mechanisms of liver injury exist, progression of chronic liver disease follows a common pathway of liver inflammation, injury and fibrosis[2]. Here we examined the association between clonal haematopoiesis of indeterminate potential (CHIP) and chronic liver disease in 214,563 individuals from 4 independent cohorts with whole-exome sequencing data (Framingham Heart Study, Atherosclerosis Risk in Communities Study, UK Biobank and Mass General Brigham Biobank). CHIP was associated with an increased risk of prevalent and incident chronic liver disease (odds ratio = 2.01, 95% confidence interval (95% CI) [1.46, 2.79]; $P < 0.001$). Individuals with CHIP were more likely to demonstrate liver inflammation and fibrosis detectable by magnetic resonance imaging compared to those without CHIP (odds ratio = 1.74, 95% CI [1.16, 2.60]; $P = 0.007$). To assess potential causality, Mendelian randomization analyses showed that genetic predisposition to CHIP was associated with a greater risk of chronic liver disease (odds ratio = 2.37, 95% CI [1.57, 3.6]; $P < 0.001$). In a dietary model of non-alcoholic steatohepatitis, mice transplanted with *Tet2*-deficient haematopoietic cells demonstrated more severe liver inflammation and fibrosis. These effects were mediated by the NLRP3 inflammasome and increased levels of expression of downstream inflammatory cytokines in *Tet2*-deficient macrophages. In summary, clonal haematopoiesis is associated with an elevated risk of liver inflammation and chronic liver disease progression through an aberrant inflammatory response.

Chronic liver disease affects more than 30% of Americans in an age-dependent fashion[3]. Chronic liver disease is characterized by an inflammatory and fibrotic response to an initial insult, most commonly steatosis from excess alcohol consumption, obesity or viral hepatitis[4], which progresses along a spectrum of histopathologic changes from liver fat accumulation (steatosis) to liver inflammation and hepatocyte ballooning injury (steatohepatitis), fibrosis and cirrhosis. However, the factors that influence progression from steatosis to inflammation and fibrosis are poorly understood.

Liver inflammation and fibrosis are mediated in part by non-parenchymal cells of the liver, including sinusoidal endothelial cells, dendritic cells, lymphocytes and macrophages.

Resident liver macrophages (Kupffer cells) and bone marrow-derived monocytes and macrophages have been implicated in responses to liver injury in both mouse models and humans[5,6]. In non-alcoholic fatty liver disease, macrophage recruitment is required for progression to non-alcoholic steatohepatitis (NASH), whereas inhibition of monocyte recruitment prevents disease progression in mouse models[7,8,9]. Furthermore, monocyte-derived inflammatory macrophages are enriched in liver samples from patients who progress from NASH to cirrhosis[8].

Dysregulated inflammatory responses in macrophages and other inflammatory cells can occur in the setting of CHIP, which is characterized by the expansion of haematopoietic cells bearing oncogenic somatic mutations most frequently in the genes *DNMT3A*, *TET2* and *ASXL1*[10]. Whole-exome sequence analysis of blood DNA has led to the recognition that CHIP is a common phenomenon with increasing prevalence in older age, present in greater than 10% of people over 70 years old[11,12,13]. CHIP is associated with future risk of haematologic malignancy[11,13], all-cause mortality[11,13] and atherosclerotic cardiovascular disease[14,15]. Mouse models have revealed the proinflammatory role of macrophages derived from mutant CHIP clones and their contributions to atherogenesis[14,16,17]. Given the pervasive nature of circulating immune cells, we reasoned that CHIP could potentially influence the trajectory of steatohepatitis and cirrhosis through aberrant inflammation in the liver.

Here we test the hypothesis that CHIP is a risk factor for chronic liver disease by: associating CHIP with independent risk of chronic liver disease in four distinct cohorts; associating CHIP with subclinical advanced liver imaging biomarkers; causal inference with human germline genetics; causal inference in mouse models; and mechanistic inference using mouse models and human germline genetics.

CHIP association with liver disease

We examined whether CHIP is associated with an elevated risk of chronic liver disease, ascertained using clinician interview and International Classification of Diseases (ICD) codes in three cohorts (Table 1 and Supplementary Table 1). We tested the association of CHIP with prevalent chronic liver disease using data from the Framingham Heart Study (FHS, n = 4,230) and the Atherosclerosis Risk in Communities (ARIC, n = 7,414) study. We tested the association of CHIP with incident chronic liver disease using the subsample of the UK Biobank for which whole-exome sequencing had been carried out (n = 201,409) as well as the subsample of the UK Biobank for which array genotyping was carried out (n = 239,316). In these cohorts, the mean age range was 57–61 years and the standard deviation was 6–16 years. The prevalence of CHIP, ascertained by exome sequencing, varied between 4% and 9% (Table 1). As in previous cohorts, *DNMT3A* and *TET2* were the most commonly mutated genes in CHIP (40%; Extended Data Fig. 1a). The prevalence of CHIP increased across cohorts with increasing age (Extended Data Fig. 1b). Known associations with CHIP, including age, sex, type 2 diabetes mellitus, smoking and self-reported ethnicity, showed similar associations to CHIP across cohorts (Supplementary Table 2). In the UK Biobank, CHIP variants ascertained through genotyping (Supplementary Table 3) had a high positive predictive value for exome sequencing-ascertained CHIP (90%), showed similar

association with age to CHIP ascertained by exome sequencing (odds ratio (OR) = 1.04 per year; $P < 0.001$) and were strongly associated with incident myeloid haematologic malignancy (hazard ratio (HR) = 106, 95% CI [72, 158]; $P < 0.001$).

In FHS, individuals with CHIP with a variant allele fraction ≥ 10% ($CHIP_{\geq 10\%}$) were at increased odds of prevalent chronic liver disease after adjustment for age, sex, type 2 diabetes and smoking (OR = 3.47, 95% CI [1.60, 7.51]; $P = 0.0016$; Fig. 1a). The association between CHIP and chronic liver disease in ARIC alone did not reach statistical significance (OR = 1.52, 95% CI [0.47, 4.93]; $P = 0.46$), nor did a cross-sectional analysis of UK Biobank data (OR = 1.16, 95% CI [0.61, 2.20]; $P = 0.63$; Supplementary Table 4). A fixed-effects model combining FHS and ARIC demonstrated a statistically significant association between CHIP and prevalent chronic liver disease (OR = 2.70, 95% CI [1.42, 5.16]; $P = 0.002$; Fig. 1a). A meta-analysis of a cross-sectional cohort of individuals from UK Biobank, ARIC and FHS showed a significant effect of CHIP on risk of prevalent NASH (OR = 1.87, 95% CI [1.17, 3.01]; $P = 0.008$). In the UK Biobank, individuals with CHIP≥10% demonstrated increased risk for incident chronic liver disease (HR = 1.82, 95% CI [1.25, 2.65]; $P = 0.001$) over a mean follow-up duration of 8.1 years (Fig. 1a and Supplementary Table 4). After excluding 39 cases of incident chronic liver disease that occurred within 1 year of enrolment, CHIP continued to be associated with incident chronic liver disease (HR = 1.53, 95% CI [1.02, 2.30]; $P = 0.038$). Overall, $CHIP_{\geq 10\%}$ was associated with a twofold increased risk of prevalent or incident chronic liver disease (OR = 2.01, 95% CI [1.46, 2.79]; $P < 0.001$; Fig. 1a). No evidence of heterogeneity was observed between estimates among cohorts or estimates between prevalent and incident chronic liver disease ($\tau^2 = 0.1012$; $P = 0.17$). Individuals with CHIP continued to be at elevated risk of chronic liver disease after adjusting for baseline alcohol consumption, body mass index, alanine transaminase levels, aspartate transaminase levels and alkaline phosphatase levels (OR = 2.11, 95% CI [1.80, 2.47]; $P < 0.001$). When interaction terms between CHIP status, current smoking and alcohol consumption in weekly drinks were included in the model, there was no statistically significant interaction between current smoking ($p_{\text{interaction}} = 0.48$) or alcohol consumption in weekly drinks ($p_{\text{interaction}} = 0.95$).

CHIP with variant allele fraction < 10% was not significantly associated with chronic liver disease (OR = 1.28, 95% CI [0.75, 2.19]; $P = 0.37$; Extended Data Fig. 2a). *JAK2*-mutant CHIP was associated with a highly elevated risk of chronic liver disease (OR = 17.65, 95% CI [4.32, 72.15]; $P < 0.001$), potentially due to established prothrombotic effects; nevertheless, non-*JAK2*-mutant CHIP was also associated with an elevated risk of chronic liver disease (OR = 1.88, 95% CI [1.09, 3.24]; $P = 0.02$; Extended Data Fig. 2b). *TET2*-mutant CHIP was independently associated with an elevated risk of chronic liver disease (OR = 5.35, 95% CI [2.22, 12.93]; $P < 0.001$; Extended Data Fig. 2b). Using Firth's logistic regression for low exposure counts provided similar estimates. *JAK2*-mutated CHIP was associated with a 16-fold increased risk of chronic liver disease (OR = 15.9, 95% CI [4.7, 54.4]; $P = 1 \times 10^{-5}$), non-*JAK2*-mutated CHIP was associated with a twofold increased risk of chronic liver disease (OR = 2.0, 95% CI [1.2, 3.4]; $P = 0.01$), and *TET2*-mutated CHIP was associated with a fivefold increased risk of chronic liver disease (OR = 5.5, 95% CI [2.4, 12.7]; $P = 8 \times 10^{-5}$). Autosomal chromosomal mosaicism of blood cells, a form of

clonal haematopoiesis that is distinct from CHIP[18], was not significantly associated with chronic liver disease risk in the UK Biobank (OR = 1.18, 95% CI [0.97, 1.45]; $P = 0.10$).

We next examined cumulative risk of chronic liver disease in the UK Biobank by array-derived CHIP status. Individuals without CHIP had a 1% cumulative incidence of chronic liver disease by the age of 80 years. By contrast, individuals with CHIP had a 6% cumulative incidence of liver disease ($P < 0.001$; Extended Data Fig. 2c,d). In comparison, individuals with morbid obesity (body mass index > 35 kg m^{-2}) without CHIP had a 2.5% cumulative incidence of liver disease. Mutual modelling of CHIP and clinical risk factors of chronic liver disease showed that CHIP association with chronic liver disease is comparable to that of well-known risk factors, such as obesity (Supplementary Table 5).

We next examined cumulative risk of chronic liver disease in the UK Biobank by array-derived CHIP status. Individuals without CHIP had a 1% cumulative incidence of chronic liver disease by age 80 years. In contrast, individuals with CHIP had a 6% cumulative incidence of liver disease (p<0.001, Extended Data Fig. 2c-d). In comparison, individuals with morbid obesity (BMI > 35 kg/m^2) without CHIP had a 2.5% cumulative incidence of liver disease. Mutual modeling of CHIP and clinical risk factors of chronic liver disease showed that CHIP association with chronic liver disease is comparable to that of well-known risk factors, such as obesity (Supplementary Table 5).

When the subtypes of liver disease were examined, individuals with CHIP were at significantly elevated risk of NASH (OR = 1.81, 95% CI [1.23, 2.68]; P = 0.0028; Fig. 1b and Supplementary Table 6) but not alcohol-related liver disease (OR = 1.74, 95% CI [0.92, 2.20]; $P = 0.089$; Fig. 1b). Only seven individuals with virus-related chronic liver disease (chronic liver disease and a history of hepatitis C or hepatitis B) could be identified, preventing ascertainment of the association of CHIP with viral hepatitis-related chronic liver disease. To further confirm the association of CHIP with NASH, we identified 114 individuals with biopsy-proven NASH and 1,368 matched controls in the Mass General Brigham (MGB) Biobank (Supplementary Table 7). Patients with biopsy-proven NASH were four times as likely to have CHIP as control subjects (OR = 3.99, 95% CI [1.24, 12.84]; $P = 0.02$; Fig. 1c).

Causality of CHIP and liver disease

To assess whether the association of CHIP status with chronic liver disease is causal, we carried out Mendelian randomization analysis. We identified 184 independent genetic variants associated with CHIP status at $P < 0.0001$ significance from a recent genome-wide association study (GWAS) comprising 97,691 blood DNA-derived whole-genome sequences[19] (Supplementary Table 8). We tested the association of these variants with cirrhosis risk using summary statistics from a GWAS of 5,770 cirrhosis cases and 487,780 controls[20]. Using the Mendelian randomization with robust adjusted profile score (MR-RAPS) method, which increases power to detect a significant effect of genetic predisposition to CHIP and accounts for potential directional pleiotropy, CHIP was associated with a twofold increased risk of chronic liver disease (OR = 2.37, 95% CI [1.57, 3.6]; $P < 0.001$; Fig. 1d). This estimate did not differ significantly from the observational estimate ($p_{\text{interaction}}$

= 0.78). Similar estimates were obtained in sensitivity analyses using the pleiotropy-robust Mendelian randomization methods MR-median regression and MR-PRESSO, multivariate MR, and MR-RAPS with varying *P*-value thresholds for inclusion of instrumental SNPs (Supplementary Table 9).

MR-Egger regression demonstrated a larger effect estimate compared to all other analyses and exhibited a significant non-zero intercept ($P = 0.008$) suggestive of directional pleiotropy; that is, certain genetic variants may exert direct effects on chronic liver disease regardless of their associations with CHIP (Extended Data Fig. 3a and Supplementary Table 9). Potentially pleiotropic genetic variants that are associated with body mass index, type 2 diabetes, lipid levels, blood pressure, current smoking and alcohol consumption, and other confounders were specifically excluded from MR-RAPS analysis with similar estimates (Supplementary Tables 9 and 10). Nevertheless, it remains likely that alternative causal pathways can impact CHIP and chronic liver disease in parallel, potentially through common mechanisms in responding to inflammatory stimuli in both settings. To further demonstrate specificity of the MR framework for CHIP, we carried out a phenome-wide Mendelian randomization analysis across twenty-two phenotypes, including risk factors for cardiac conditions, autoimmune diseases and solid malignancies. Apart from CHIP association with chronic liver disease, we did not observe any additional significant associations in this analysis, suggesting that the association between CHIP and chronic liver disease is specific (Extended Data Fig. 3b). As confirmation of the robustness of the MR-RAPS framework, genetic predisposition to CHIP was significantly associated with the development of myeloproliferative neoplasms (OR = 39.4, 95% CI [5.2, 188.0]; $P < 0.001$), consistent with the known association between CHIP and haematologic malignancies[11,21]. By contrast, MR-Egger did not demonstrate a significant intercept term for myeloproliferative neoplasm (OR = 30.8, 95% CI [9.8, 51.8]; $P = 0.004$).

Association with liver imaging and biomarkers

We studied whether CHIP may be associated with increased liver inflammation and fibrosis using magnetic resonance imaging data from 8,251 individuals in the UK Biobank. CHIP was associated with increased likelihood of liver inflammation and fibrosis (iron-corrected T1 relaxation time (cT1) ≥ 795 ms; OR = 1.74, 95% CI [1.16, 2.60]; $P = 0.007$) but was not significantly associated with hepatic steatosis (proton density fat fraction ≥ 5%, OR = 0.98, 95% CI [0.75, 1.28]; $P = 0.89$; Fig. 2a,b). Using data from the UK Biobank, we also examined the relationship between CHIP and serum biomarkers in up to 393,128 individuals (Extended Data Fig. 4a). There were no statistical associations between CHIP and alanine transaminase levels or aspartate transaminase levels, but CHIP was significantly associated with a modest increase in γ-glutamyl transferase (1.1 U l^{-1}; $P = 0.0062$). CHIP was also associated with a modest elevation in platelet count (6,500 per microlitre; $P < 0.001$) and leukocyte count (0.21×10^9 cells l^{-1}; $P = 0.01$). When *JAK2* CHIP was excluded, CHIP continued to be associated with elevations in platelet and leukocyte counts and γ-glutamyl transferase (Extended Data Fig. 4b). When TET2 CHIP was excluded, CHIP continued to be associated with increased platelet and leukocyte counts, but not with γ-glutamyl transferase (Extended Data Fig. 4c).

Tet2$^{-/-}$ hematopoiesis promotes steatohepatitis

To examine whether *Tet2* deficiency has a role in chronic liver inflammation, we utilized mouse models of steatohepatitis in which fatty liver and chronic inflammation are induced by diet. Choline-deficient, L-amino acid-defined, high-fat diet (CDAHFD) disrupts hepatic mitochondrial β-oxidation and production of very low-density lipoprotein, resulting in liver oxidative damage, chronic liver injury and elevated serum aminotransferases[22,23] (Extended Data Fig. 5). B6.SJL mice were transplanted with *Tet2*$^{-/-}$ or control bone marrow cells and fed CDAHFD for 11 weeks, after which liver fat, inflammation and hepatocyte ballooning injury were assessed histologically and integrated into a modified non-alcoholic fatty liver disease activity score (NAS; Supplementary Table 11). Mice transplanted with *Tet2*$^{-/-}$ haematopoietic cells consumed less CDAHFD daily (although this difference was not statistically significant) and showed slightly reduced hepatomegaly (Extended Data Fig. 5). Lower dietary intake notwithstanding, *Tet2*$^{-/-}$-transplanted mice demonstrated similar liver fat accumulation and serum metabolic and haematologic parameters to those of control-transplanted mice (Extended Data Figs. 5 and 6). By contrast, *Tet2*$^{-/-}$-transplanted animals showed more lobular inflammation with prominent lymphoid aggregates and hepatocyte ballooning, but liver fat accumulation was not affected (Fig. 2c-f). Overall, these changes corresponded to higher cumulative NAS (Fig. 2g). Supporting the histologic findings, bulk liver mRNA from *Tet2*$^{-/-}$-transplanted mice showed enrichment in transcriptional programs associated with steatohepatitis and liver fibrosis (Extended Data Fig. 7a). These findings demonstrate that *Tet2*$^{-/-}$ haematopoietic cells promote the development of steatohepatitis in mice.

Similar findings of increased liver inflammation and increased hepatocyte damage were observed in hypercholesterolemic *Ldlr*$^{-/-}$ mice transplanted with *Tet2*$^{-/-}$ bone marrow cells and fed Western diet (Extended Data Fig. 7b-g). Furthermore, transplantation of haematopoietic cells lacking *Dnmt3a*, the most commonly mutated gene in CHIP, also led to increased liver inflammation and higher aggregate NAS in CDAHFD-fed mice (Extended Data Fig. 7h). Therefore, we found that mutant haematopoietic cells lacking *Tet2* or *Dnmt3a* aggravate chronic liver injury in different dietary and genetic models that promote steatohepatitis.

To study the persistence of liver injury in the setting of mutant haematopoiesis, *Tet2*$^{-/-}$-transplanted animals were fed CDAHFD for 11 weeks and subsequently fed standard chow for 10 days. We observed a global decrease in steatohepatitis after diet reversion, reflected in lower NAS scores. Nevertheless, unlike liver fat, liver inflammation and hepatocyte ballooning injury remained statistically significantly higher in *Tet2*$^{-/-}$-transplanted mice compared to wild-type controls (Extended Data Fig. 7i). These findings suggest that persistent liver inflammation and injury mediated by *Tet2*$^{-/-}$ haematopoietic cells may promote chronic liver disease in the setting of repeated liver insults[24]. Persistent liver inflammation can also stimulate inflammatory scarring and fibrosis of the liver[6]. Although liver fibrosis gene signatures were enriched in *Tet2*$^{-/-}$-transplanted mice (Extended Data Fig. 7a), significant liver fibrosis was not observed histologically in *Tet2*$^{-/-}$- and control-transplanted animals after 11 weeks of CDAHFD (Extended Data Fig. 7g). Therefore, mice were diet-fed for an extended duration. At 19 weeks, *Tet2*$^{-/-}$-transplanted mice showed

significantly increased liver fibrosis compared to that of wild-type controls (Fig. 2h). This finding demonstrates that haematopoietic loss of *Tet2* promotes the progression of steatohepatitis to liver fibrosis in CDAHFD-fed mice.

Tet2$^{-/-}$ macrophages mediate liver injury

To identify the cell lineages in *Tet2*-deficient haematopoiesis that contribute to NASH progression, we carried out in vitro experiments in which wild-type hepatic stellate cells were grown in the presence of purified haematopoietic cell populations from *Tet2*$^{-/-}$ and wild-type control mice. RNA sequencing of hepatic stellate cells co-cultured with hepatic macrophages specifically showed transcriptional upregulation of genes known to be involved in the fibrogenic activation of hepatic stellate cells, such as *Col4a1*, *Col4a2*, *Lox*, *Loxl2* and *Timp1* (Extended Data Fig. 8a). Gene set enrichment analysis confirmed that direct co-culture with wild-type or *Tet2*$^{-/-}$ hepatic macrophages, Transwell culture with *Tet2*$^{-/-}$ hepatic macrophages and direct culture with *Tet2*$^{-/-}$ B cells led to a significant enrichment of gene signatures characteristic of hepatic stellate cell activation (Extended Data Fig. 8b). Therefore, hepatic macrophages are an important haematopoietic cell type in promoting the liver's fibrogenic response, either directly or, more likely, by means of increased inflammatory signals.

Liver-resident phagocytes, namely Kupffer cells, are a major source of proinflammatory cytokine secretion in response to immune stimuli and inflammasome activation. After haematopoietic transplant, Kupffer cells, which express F4/80^{+}CD11b^{mod}, are replaced by donor-derived cells expressing the CD45.1 congenic marker[25,26] (Extended Data Fig. 9a). Subsequent feeding with CDAHFD promotes the accumulation of donor-derived F4/80^{mod}CD11b^{hi} hepatic macrophages, which form crown-like structures in the liver (Extended Data Fig. 9b). Compared to wild-type cells, *Tet2*$^{-/-}$ hepatic macrophages in bone marrow-transplanted, CDAHFD-fed mice showed increased levels of expression of *Il6* and *Cxcl1* (Fig. 3a) as well as enrichment in proinflammatory gene signatures (Extended Data Fig. 9c). Serum levels of interleukin-6 (IL-6), CXCL1, CCL22 and CCL17 were also increased in mice transplanted with *Tet2*$^{-/-}$ bone marrow (Fig. 3b). CXCL1 and IL-6 are proinflammatory molecules regulated by the NLRP3 inflammasome complex, whereas the related chemokines CCL17 and CCL22 signal through CCR4 to promote the recruitment of regulatory T cells[27]. Confirming the key role of NLRP3 in mediating downstream proinflammatory cytokine secretion, bone marrow-derived macrophages lacking *Tet2* showed increased secretion of IL-6, CXCL1, CCL22 and CCL17, whereas cells lacking both *Tet2* and *Nlrp3* showed baseline expression levels (Fig. 3c). Therefore, haematopoietic *Tet2* loss exerts a proinflammatory effect in macrophages through downstream cytokine secretion in an NLRP3-dependent fashion. Furthermore, mice transplanted with *Tet2*$^{-/-}$*Nlrp3*$^{-/-}$ bone marrow and fed CDAHFD for 11 weeks showed significantly reduced liver inflammation and hepatocyte ballooning compared to *Tet2*$^{-/-}$-transplanted mice, resulting in overall lower NAS (Fig. 2c,g). Together, these findings support a model in which *Tet2*-deficient haematopoiesis induces NLRP3-dependent proinflammatory signals in liver-resident immune cells to promote steatohepatitis and fibrosis.

Previous work had revealed that a damaging IL-6 receptor gene (*IL6R*) missense variant (p.Asp358Ala, rs2228145) is associated with greater protection from coronary artery disease in humans with CHIP[15]. Therefore, we examined whether this variant is also associated with protection from chronic liver disease among individuals with CHIP compared to those without CHIP. We observed a significant interaction in the association of p.Asp358Ala with chronic liver disease by CHIP status ($p_{interaction}$ = 0.02). Among individuals without CHIP, there was no significant association between p.Asp358Ala and chronic liver disease risk (OR = 1.07, 95% CI [0.92, 1.25]; P = 0.4). By contrast, p.Asp358Ala protected against chronic liver disease among individuals with CHIP (OR = 0.44, 95% CI [0.21, 0.93]; P = 0.03; Fig. 3a). This finding implicates proinflammatory IL-6 signalling in the contribution of CHIP to chronic liver disease.

Discussion

By combining large-scale human genetic studies with in vivo modelling of clonal haematopoiesis in mouse models, we demonstrate that CHIP is associated with an elevated risk of chronic liver disease, including NASH, via aberrant inflammatory responses. The overall nearly twofold increased risk of incident chronic liver disease observed in the current study is comparable to the nearly twofold increased risk of incident coronary artery disease previously reported with CHIP in overlapping cohorts[14,15]. Mendelian randomization and mouse studies support a causal role for CHIP in the pathogenesis of chronic liver disease. Furthermore, Mendelian randomization analyses and in vivo inflammatory biomarker and transcriptional analyses implicate the NLRP3 inflammasome and downstream IL-6 activity in CHIP-associated chronic liver disease.

Our findings support a model of CHIP promoting steatohepatitis particularly among individuals with elevated liver fat or other sources of liver injury that increase cirrhosis risk[24]. First, individuals with CHIP showed higher indices of liver inflammation and fibrosis with no significant difference in liver fat accumulation. Second, haematopoietic-specific *Tet2* inactivation increased the severity of diet-induced steatohepatitis in mice owing to increased liver inflammation, hepatocyte ballooning injury and fibrosis, without apparent influence on liver fat. Unlike germline genetic variants that predispose to both liver fat and cirrhosis[20], CHIP tends to exaggerate the proinflammatory response to a present stimulus, which in the setting of NASH results in enhanced activation of local immune and fibrogenic pathways in the fatty liver. Haematopoietic loss of *Tet2* also causes glucose intolerance[28], a significant risk factor for NASH progression due to increased oxidative and inflammatory stress.

We also provide human genetic evidence for a potential causal relationship between CHIP and liver disease. Mendelian randomization analysis is useful for distinguishing between outcomes that may be caused by CHIP and those from other confounding associations. To optimize statistical power in the setting of low heritability of CHIP[19], we applied a Mendelian randomization technique (MR-RAPS) that allows for the use of subgenome-wide significant variants[29]. We observed that germline genetic predisposition to CHIP predisposes to chronic liver disease risk. Therefore, CHIP is probably a causal risk factor for chronic liver disease. Consequently, targeting factors that promote CHIP-associated liver injury as

well as targeting CHIP itself are both expected to reduce the risk of chronic liver disease among susceptible individuals.

Genetic deficiency of IL-6 signalling due to the presence of *IL6R* p.Asp358Ala in CHIP individuals was associated with a greater reduction in chronic liver disease risk, but not among those without CHIP. This finding is compatible with our previous observation that the presence of *IL6R* p.Asp358Ala was associated with a markedly reduced risk for incident cardiovascular disease risk, but not haematologic malignancy, specifically among individuals with CHIP[15]. In the current study, we observed increased serum IL-6 levels in mice transplanted with *Tet2*$^{-/-}$ bone marrow; furthermore, *Tet2*$^{-/-}$ liver macrophages also showed increased expression of IL-6 and other proinflammatory cytokines and chemokines with important roles in chronic liver disease. The role of IL-6 in steatohepatitis is complex, with dual activity in the acute-phase response and liver regeneration[30,31]. In addition, we have demonstrated that steatohepatitis is further modulated by bone marrow inflammatory cells, which exhibit increased IL-6 inflammatory activity in the absence of *Tet2*. This process requires the upstream regulator NLRP3, which is recognized as a central hub of the inflammatory immune response in hepatic parenchymal and non-parenchymal cells[32,33,34]. Considering the heterogeneous nature of the cell types involved, broad pharmacologic inhibition of the NLRP3 inflammasome[32] is one potential strategy for modifying liver inflammation and fibrosis in CHIP. Although liver toxicity has been reported with use of the NLRP3 inhibitor MCC950, raising particular concern in this group of patients, we suggest that NLRP3 inhibition may be protective against liver injury in susceptible CHIP individuals in whom the NLRP3-dependent inflammatory input is exaggerated specifically in haematopoietic cells. Further in vivo and preclinical testing will be required to determine safety.

In conclusion, CHIP is associated with an elevated risk of chronic liver disease specifically through the promotion of liver inflammation and injury. Through targeting of the NLRP3 inflammasome or downstream mediators, CHIP may be a modifiable risk factor for chronic liver disease.

Methods

Study samples

Secondary analysis of data from clinical studies involving human participants was approved by the MGB Institutional Review Board. We examined the association between CHIP and chronic liver disease using five datasets. For analysis of prevalent disease, we used data from the FHS (n = 4,114) and ARIC (n = 7,414; Table 1) studies. For analysis of incident disease, we tested the association of CHIP and genotyped CHIP variants with incident chronic liver disease in distinct groups of individuals from the UK Biobank who underwent whole-exome sequencing (n = 201,409) and a separate subsample of individuals from the UK Biobank who underwent array-based genotyping using genotyped CHIP variants (n = 239,316). Only a subset of CHIP variants were available on the genotyped UK Biobank array (Supplementary Table 3). Individuals with prevalent leukaemia or other haematologic malignancy were excluded from analysis. All patients with whole-exome sequencing data

from FHS, ARIC and the UK Biobank were included in the analysis. Median duration of follow up for incident disease analysis was 8.1 years.

We defined chronic liver disease as the development of liver fibrosis or cirrhosis, combining the following ICD10 diagnostic codes: K70.2 (alcoholic fibrosis and sclerosis of the liver), K70.3 (alcoholic cirrhosis of the liver), K70.4 (alcoholic hepatic failure), K74.0 (hepatic fibrosis), K74.1 (hepatic sclerosis), K74.2 (hepatic fibrosis with hepatic sclerosis), K74.6 (other and unspecified cirrhosis of liver), K76.6 (portal hypertension) and I85 (oesophageal varices). These ICD codes have previously been demonstrated to have high specificity for identification of patients with cirrhosis compared to physician review and associate strongly with known cirrhosis loci[20].

In addition to examining all-cause chronic liver disease, we also examined the association of CHIP with subtypes of chronic liver disease. Non-alcoholic fatty liver disease was defined as chronic liver disease among individuals consuming fewer than 21 drinks per week for men and fewer than 14 drinks per week for women and no history of hepatitis B or hepatitis C as outlined in the American Association for the Study of Liver Diseases guidelines[35]. Alcohol-related liver disease was defined as chronic liver disease among individuals with excess alcohol intake (≥21 drinks per week for men or ≥14 drinks per week for women) and no history of hepatitis B or hepatitis C. Seven individuals with liver disease and a known history of hepatitis B or hepatitis C were excluded from the analysis of CHIP association with subtypes of chronic liver disease.

As the above analyses of chronic liver disease were based primarily on ICD10 codes, we also examined whether CHIP predisposes to biopsy-proven NASH (n = 1,482). For this analysis, we analysed 114 individuals with biopsy-proven NASH and 1,368 control individuals in the MGB Biobank matched for age, sex, type 2 diabetes, body mass index and smoking.

To examine whether CHIP is associated with serum biomarker levels or liver imaging findings, we used data from the UK Biobank. Blood samples were collected from all UK Biobank participants during their initial enrolment visit. These samples were used for both whole-exome sequencing and for biomarker assays. In a cross-sectional analysis, we tested the association between CHIP and inverse-normal-transformed values of serum liver enzyme levels (alanine transaminase levels, aspartate transaminase levels, alkaline phosphatase levels and γ-glutamyl transferase levels) and serum inflammatory biomarkers (C-reactive protein, platelet count, haemoglobin and white blood cell count). Serum liver enzyme levels and C-reactive protein were measured by immunoassay using a Beckman Coulter AU5800 analyser. Blood cell counts were measured using a Beckman Coulter LH 750 analyser.

We examined whether CHIP status was associated with liver fat and/or liver inflammation and fibrosis in 4,434 individuals in the UK Biobank with whole-exome sequencing data who underwent MultiScan magnetic resonance imaging of their liver[36]. Liver fat was measured using the proton density fat fraction. The likelihood of liver inflammation and fibrosis was measured using cT1[36].

Whole-exome sequencing and CHIP ascertainment

Whole-exome sequences from 7,414 individuals in ARIC were obtained from dbGAP (accession phs000280). DNA from ARIC was obtained from whole-blood samples at the time of study enrolment. For FHS, exome sequencing was carried out as part of the Trans-Omics for Precision Medicine (TOPMed) programme. In the UK Biobank, whole-exome sequencing was carried out centrally at the Regeneron Genetics Center. We analysed 201,309 whole exomes from unrelated individuals in the UK Biobank. CHIP in MGB Biobank participants was ascertained through whole-exome sequencing of blood samples deposited at the time of enrolment. Individuals with prevalent leukaemia or other haematologic malignancy were excluded from analysis.

We identified individuals with CHIP on the basis of a prespecified list of variants in 74 genes that are recurrently mutated in myeloid cancers (Supplementary Table 12). For analyses of FHS and ARIC cohorts for prevalent liver disease, CHIP was ascertained using whole-exome sequencing[15,19]. For analysis of the UK Biobank cohort for incident liver disease, CHIP was ascertained using whole-exome sequencing in the subset of individuals for whom exome sequencing data were available (n = 201,409). For the UK Biobank subset in which genotyping array data were available (n = 239,316), CHIP was ascertained using array-derived genotyped variants in *ASXL1*, *DNMT3A*, *JAK2* and *TET2* (Supplementary Table 3). We examined genotyping fidelity of each variant by manually examining imaging files with ScatterShot. Individuals included in whole-exome sequencing and prevalence analysis were excluded from this analysis. In the primary analysis, we examined CHIP with a variant allele fraction ≥10%. We analysed CHIP with a variant allele fraction below 10% separately.

Mouse models

Ldlr$^{-/-}$, B6.SJL and C57BL/6J mice at 8 weeks were exposed to 10 Gy total body irradiation and transplanted through retro-orbital injection with 1,000,000 to 2,000,000 bone marrow cells collected from sex-matched *vavCre*$^{+}$*Tet2*$^{fl/-}$, *vavCre*$^{+}$*Tet2*$^{fl/-}$*Nlrp3*$^{-/-}$, *vavCre*$^{+}$*Dnmt3a*$^{fl/-}$ or control *vavCre*$^{+}$ donor mice aged between 8 and 11 weeks. After haematopoietic reconstitution was confirmed by peripheral blood analysis and flow cytometry at 4 weeks, transplanted mice were fed an atherogenic Western diet containing 0.2% cholesterol and 42% of its kilocalories from fat (TD.88137; Envigo) or CDAHFD containing 60% of its kilocalories from fat and 0.1% methionine (A06071302; Research Diets) in non-metabolic cages for defined time periods. Mice were randomly assigned to each donor group; sample size calculations were not carried out. All animal experiments were conducted in accordance with ethical guidelines and were approved by the Institutional Animal Care and Use Committee (IACUC) at Brigham and Women's Hospital and Dana-Farber Cancer Institute.

Liver histology

Mouse livers were fixed in 10% formalin for at least 24 h. Paraffin-embedded tissue blocks were sectioned and stained using haematoxylin and eosin for blinded grading of steatohepatitis according to modified CRN criteria[37] (Supplementary Table 11). Liver

fibrosis was measured by histologic grading of Masson's trichrome staining or quantification of Picrosirius red positivity using ImageJ.

Mouse peripheral blood analysis

Peripheral blood was collected from the retro-orbital sinus into EDTA tubes. Complete blood counts were obtained using a Hemavet 950 or Heska Element HT5 analyser. After red cell lysis, cells were resuspended in PBS supplemented with 2% FBS for flow cytometric analysis. Plasma was obtained by centrifugation at 1,000*g* for 10 min at 4 °C. Cytokine levels were measured by Eve Technologies using a Luminex-based mouse cytokine–chemokine magnetic bead panel.

Cell isolation

Bone marrow cells were obtained by crushing mouse femur, tibia, pelvis and vertebrae in cold PBS containing 2% fetal bovine serum and 2 mM EDTA. The cell suspension was filtered through a 70-μm mesh filter and centrifuged at 1,200 r.p.m. for 5 min at 4 °C. After red blood cell lysis, bone marrow cells were resuspended in cold PBS containing 2% fetal bovine serum for use.

Mouse livers were perfused via the hepatic portal vein with 10 ml cold PBS followed by 5 ml of digestion mix containing 850 mg ml^{-1} collagenase I, 700 mg ml^{-1} collagenase D, 1 mg ml^{-1} Dispase II and 100 ng ml^{-1} DNase I in RPMI. After 5 min, livers were diced and agitated for 15 min in an orbital shaker at 37 °C and filtered through a 70-μm mesh filter. Parenchymal cells were removed by centrifugation at 50*g* for 2 min. The supernatant was centrifuged at 1,200 r.p.m. for 5 min, and the cell pellet was washed once with DMEM. Non-parenchymal cells were resuspended and laid on top of four OptiPrep gradients (1.085, 1.058, 1.043 and 1.034) and centrifuged in an SW-41Ti rotor at 20,000 r.p.m. for 15 min at 25 °C. Hepatic stellate cells were collected from the 1.007–1.034–1.043 interface and hepatic macrophages were collected from the 1.043–1.058 and 1.058–1.085 interfaces and further purified using negative selection by CD45 microbeads and positive selection by CD11b microbeads, respectively.

Flow cytometry/FACS

Flow cytometric analysis was carried out on a BD FACScanto II analyser; cell sorting was carried out on a Sony MA900 cell sorter. The following antibodies were used: rat anti-mouse CD3 PE–Cy7 or PerCP–Cy5.5 (17A2); rat anti-human/mouse CD11b APC–Cy7 (M1/70); rat anti-human/mouse CD45R/B220 PerCP–Cy5.5 or BV510 (RA3-6B2); mouse anti-mouse CD45.1 FITC or BV510 (A20); mouse anti-mouse CD45.2 PE or Pacific blue (104); rat anti-mouse F4/80 FITC (BM8); rat anti-mouse Gr1 Pacific blue (RB6-8C5); rat anti-mouse Ly6C PE–Cy7 or APC (HK1.4); rat anti-mouse Ly6G PE–Cy7 (1A8); mouse anti-mouse NK1.1 PerCP–Cy5.5 (PK136).

Cell culture

Bone marrow cells were cultured in RPMI supplemented with 10% fetal bovine serum, 100 U ml^{-1} penicillin/streptomycin and 2 mM L-glutamine. Macrophage differentiation was induced using 10 ng ml^{-1} recombinant M-CSF (Preprotech) and terminal differentiation was

confirmed by flow cytometric analysis after 8 days. Macrophages were exposed to 10 ng ml^{-1} LPS (Sigma) for 2 h and stimulated for 6 h with palmitic acid (300 μM; Sigma) or cholesterol monohydrate crystals (200 μg ml^{-1}; Sigma) prepared as previously described[38]. Culture supernatant was centrifuged at 1,000*g* for 10 min at 4 °C and cytokine levels were measured by Eve Technologies using a Luminex-based mouse cytokine–chemokine magnetic bead panel.

Hepatic stellate cells, hepatic macrophages and purified lymphocytes were cultured in RPMI supplemented with 10% fetal bovine serum, 100 U ml^{-1} penicillin–streptomycin, 2 mM L-glutamine, 1× non-essential amino acids and 0.05 mM 2-mercaptoethanol. LPS (10 ng ml^{-1}) and anti-CD3ε monoclonal antibody (145-2C11, 1 μg ml^{-1}) were used to supplement B and T lymphocyte cultures, respectively. Purified cells were grown in monocultures overnight before being directly co-cultured at 1:1 cell ratio. Hepatic macrophages were additionally grown in Transwell inserts. After 48 h, adherent cells were washed and collected for analysis.

RNA analysis

RNA from freshly perfused mouse liver or sorted liver macrophages was extracted using the Qiagen RNeasy Plus kit. Fragmentation, reverse transcription and cDNA library preparation with random hexamer primers were carried out using standard Illumina protocols. Pooled libraries were sequenced using the Illumina NovaSeq 6000. Sequenced reads were filtered to remove reads containing adapters, greater than 10% undetermined bases, or greater than 50% of bases with a Q score less than or equal to 5. Transcript abundance estimates were generated using Salmon v1.2.1 and differentially expressed genes ($\log_2$[FC] > 0.58, P_{adj} < 0.05) were identified using the R package DESeq2. Gene set enrichment analysis was carried out using GSEA v4.1.0 (Broad Institute). For sorted liver macrophages, gene sets in MSigDB C7 (filtered for macrophage-related signatures) and H (Hallmark) collections were analysed. For unsorted liver transcripts, gene sets in MSigDB C2 (filtered for liver-related signatures) and H collections were analysed, in addition to liver disease-specific gene sets extracted from published data[39,40,41]. *P* value < 0.05 and false discovery rate < 0.10 were taken to be significant.

Statistical analysis

We tested for the association of CHIP status with prevalent chronic liver disease using logistic regression, adjusting for age, sex, type 2 diabetes and smoking. Additional analyses were carried out after adjustment for alcohol consumption and body mass index. For incident analysis, we used Cox proportional hazards regression with adjustment for age, sex, type 2 diabetes and smoking. Further adjustment for alcohol consumption and body mass index was carried out as a sensitivity analysis. To aggregate the effect size of CHIP on liver disease across cohorts, inverse-variance-weighted fixed-effects meta-analysis was carried out. To test the association of CHIP status with liver imaging biomarkers, including liver fat (proton density fat fraction ≥ 5%) and liver inflammation and fibrosis (proton cT1 ≥ 795 ms), we used logistic regression with adjustment for age and sex.

To assess the causality of the association of CHIP status with chronic liver disease, we examined the association of genetic predisposition to CHIP with cirrhosis risk using Mendelian randomization. Mendelian randomization is a genetic method that assesses the causality between an exposure (CHIP) and outcome (chronic liver disease). We used MR-RAPS analysis, which provides for control of the type 1 error rate when using subgenome-wide significant genetic variants[29]. To increase statistical power to detect an effect, we used variants associated with CHIP status at a *P* value of less than 0.0001. Pruning was carried out to identify independent genetic variants using $R^2 < 0.01$ before analysis. The GWAS for the exposure (CHIP) consisted of a GWAS of CHIP status in 52 studies in the TOPMed programme. Among 97,691 individuals, 4,229 cases and 93,462 controls were analysed. Single variant association for each variant with minor allele frequency > 0.1% and minor allele count > 20 was carried out with SAIGE. Models were adjusted for age, sex and ten principal components of ancestry. The genetic variants identified exhibited strong association with CHIP (*F* statistic = 156).

We tested the association of these variants with cirrhosis risk using summary statistics from a GWAS of 5,770 cirrhosis cases and 487,780 controls[20]. This GWAS analysed all-cause cirrhosis—defined as hospitalization or death due to ICD codes K70.2, K70.3, K70.4, K74.0, K74.1, K74.2, K74.6, K76.6 or I85. Logistic regression as implemented in PLINK was used to test the association of genetic variants with all-cause cirrhosis in seven cohorts. Inverse-variance-weighted meta-analysis was used to pool estimates across all seven cohorts. All analyses were adjusted for age, sex and five principal components of ancestry. Cohorts were of European ancestry. In sensitivity analyses, we also carried out MR analysis using MR-PRESSO[42], MR-Egger[43] and multivariate MR adjusted for smoking, body mass index and type 2 diabetes[44,45,46]. No outliers were detected in the MR-PRESSO analysis. Using the MR-PRESSO global test to test for overall horizontal pleiotropy[42], no evidence of pleiotropy was observed (MR global test *P* value = 0.492). We conducted sensitivity analysis for potentially pleiotropic SNPs by specifically excluding any genetic variants that are associated with body mass index, waist-to-hip ratio adjusted for body mass index, type 2 diabetes, blood lipids, blood pressure, HbA1c level, C-reactive protein, current smoking and alcohol consumption[44,45,46,47,48,49]. To test the validity of the exchangeability assumption, we carried out MR analysis of CHIP against the potential confounders listed above (Supplementary Table 10). Reporting of MR results was carried out according to the MR-STROBE guidelines (Supplementary Table 13). Mendelian randomization analyses were conducted using the mr.raps R package and MR Base platform.

For mouse studies, pairwise comparisons were made using Student's *t*-test or the Mann–Whitney U-test as determined by normality and variance and adjusted for multiple comparisons. For comparisons between more than two groups, the chi-square test or two-way analysis of variance with post hoc Tukey's test was used. Statistical analyses were carried out in R version 3.5 or GraphPad Prism 8.3.1.

Extended Data

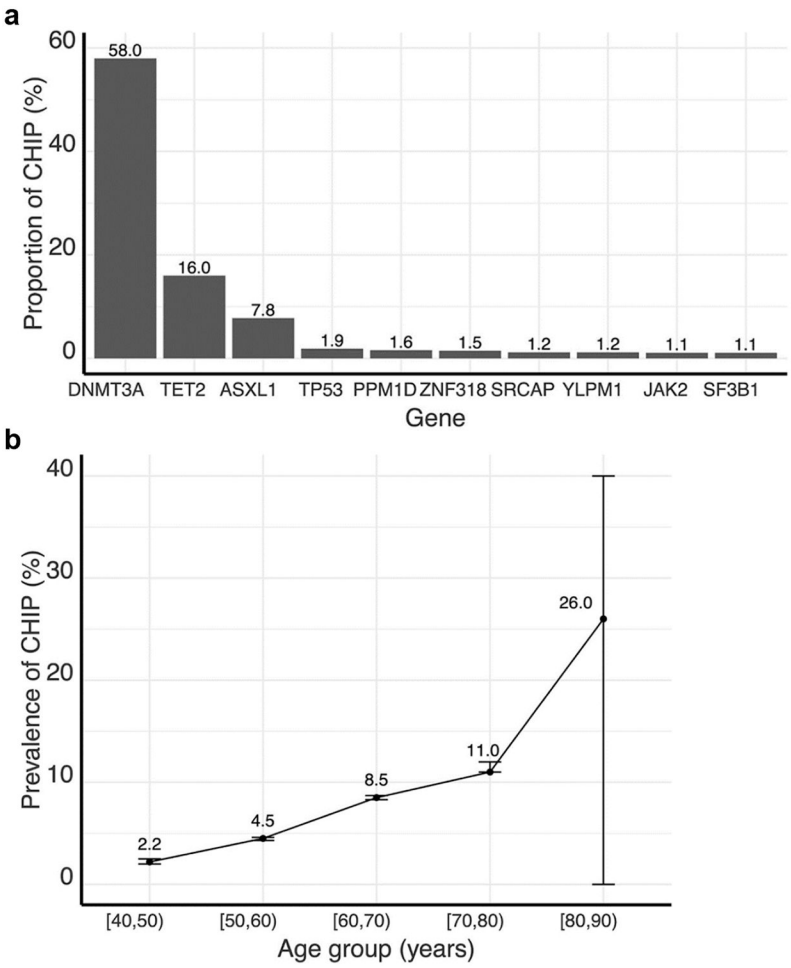

Extended Data Fig. 1. CHIP ascertainment.

a, Proportion of CHIP by mutated gene among 11,783 individuals with CHIP. **b,** Prevalence of CHIP by age.

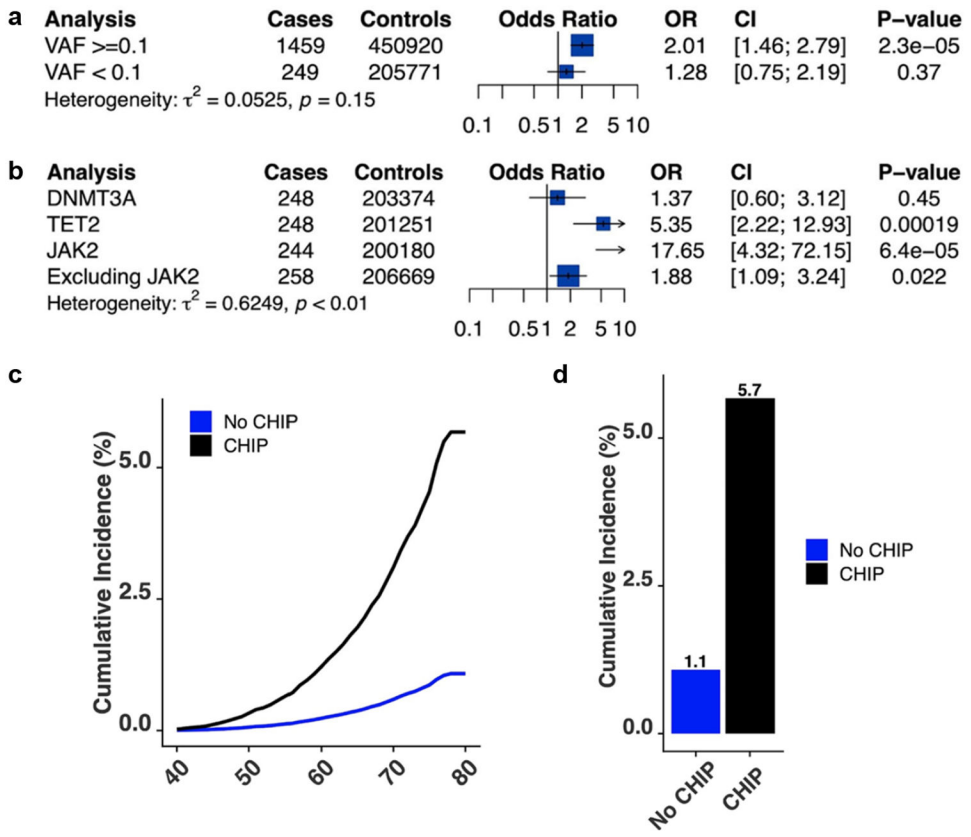

Extended Data Fig. 2. Association of CHIP with chronic liver disease.

a, Association of CHIP with prevalent or incident chronic liver disease by variant allele fraction. **b,** Association of CHIP with chronic liver disease by mutated gene. **c,** Cumulative risk of chronic liver disease by clonal hematopoiesis status in the UK Biobank. **d,** Cumulative risk of chronic liver disease by clonal hematopoiesis status in the UK Biobank by age 80 years. Estimates derived using logistic regression with adjustment for age and sex in the UK Biobank, Framingham Heart Study and Atherosclerosis Risk in Communities study and pooled using inverse variance weighted fixed effects meta-analysis. Cumulative risk of chronic liver disease by age was modeled using Cox proportional hazards model with age as the underlying time variable and adjustment for sex. CHIP, clonal hematopoiesis of indeterminate potential; CI, 95% confidence interval; OR, odds ratio; VAF, variant allele fraction.

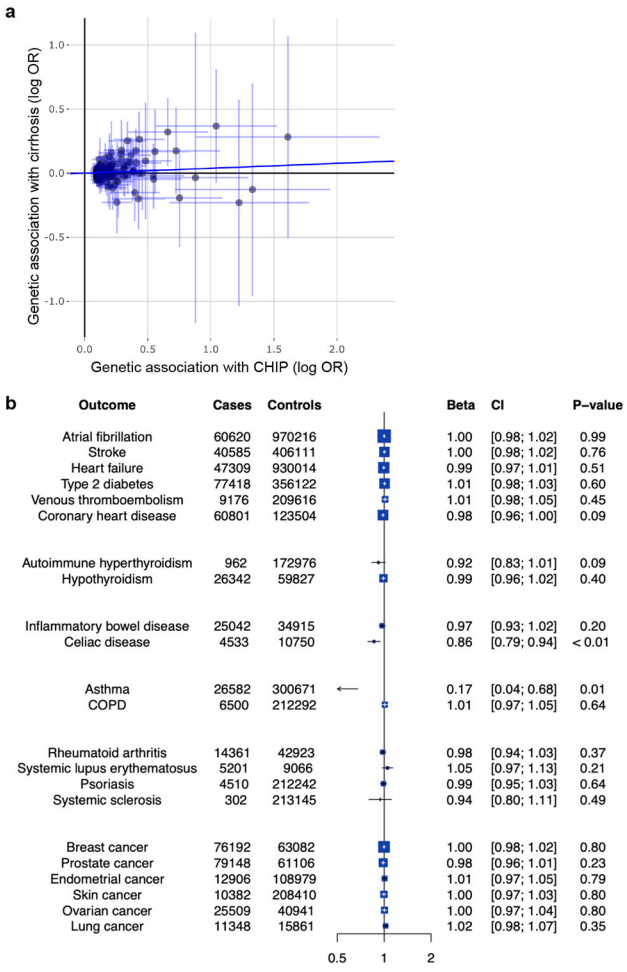

Extended Data Fig. 3. Mendelian randomization analysis of CHIP association with chronic liver disease.

a, Effect of genetic variants against exposure (CHIP) and outcome (cirrhosis). Effect estimates are oriented to CHIP-increasing alleles. **b,** Phenome-wide mendelian randomization analysis of CHIP with 22 phenotypes. MR analysis was performed using MR Base platform. Estimates were derived using inverse variance weighted meta-analysis using 90 independent variants associated with CHIP with $p < 5 \times 10^{-5}$.

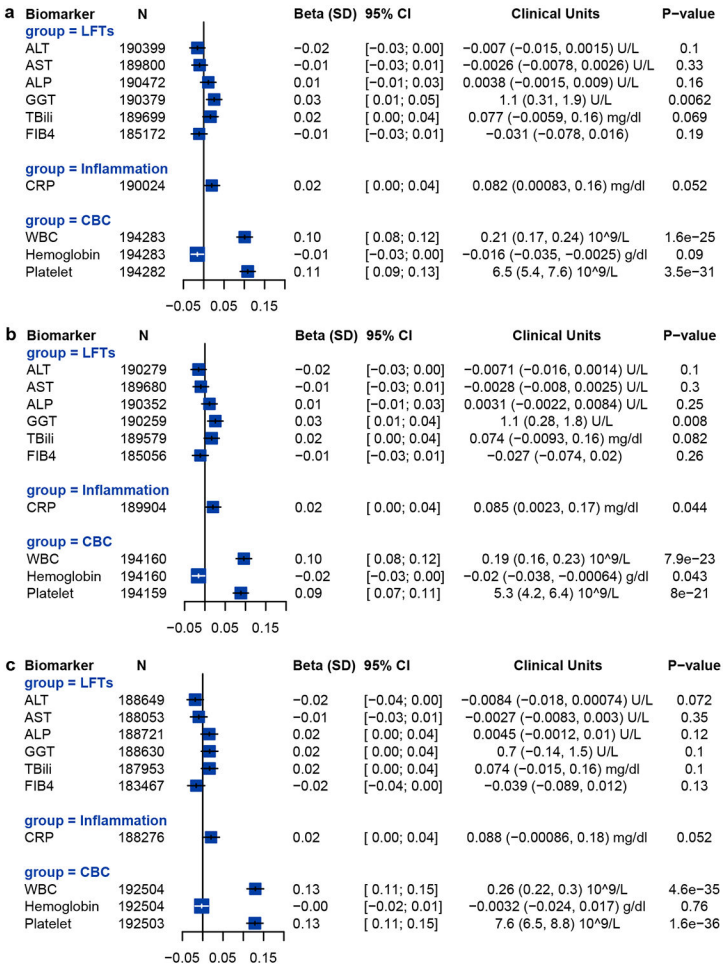

Extended Data Fig. 4. Association of CHIP with serum biomarkers.

a, Association of CHIP with serum biomarkers in the UK Biobank. **b,** Association of CHIP with serum biomarkers in the UK Biobank excluding *JAK2*-mutant CHIP. **c,** Association of CHIP with serum biomarkers in the UK Biobank excluding *TET2*-mutant CHIP. ALP, alkaline phosphatase; ALT, alanine transaminase; AST, aspartate transaminase; CHIP, clonal hematopoiesis of indeterminate potential; CRP, C-reactive protein; GGT, gamma-glutamyl transferase; TBili, total bilirubin; WBC, white blood cell count. A *P* value of 0.006 after Bonferroni adjustment (0.05/9 = 0.006) was considered significant.

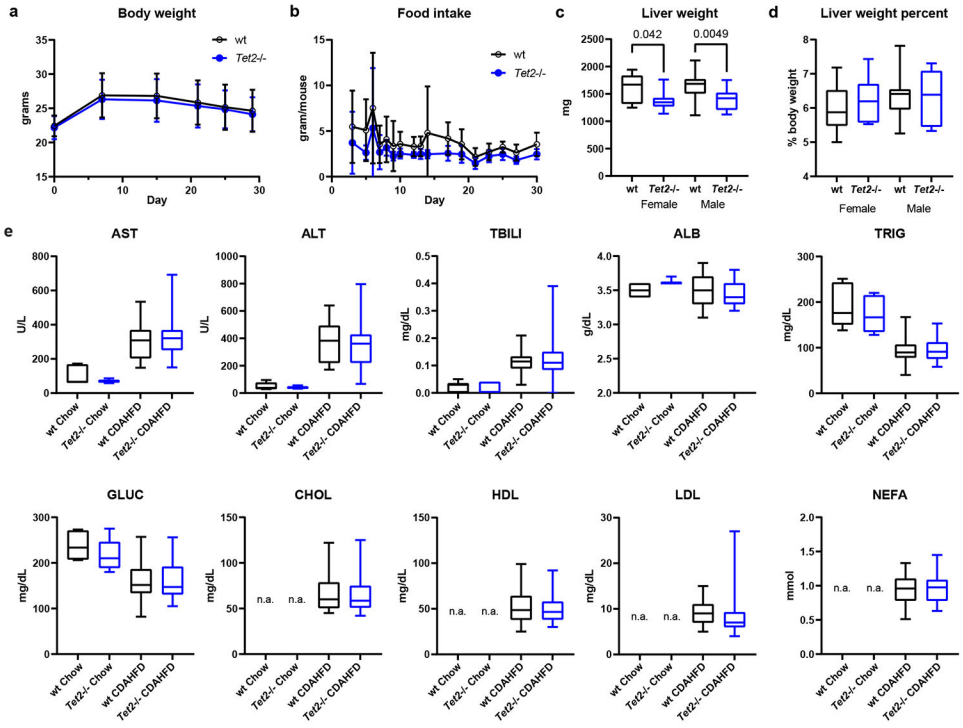

Extended Data Fig. 5. Metabolic phenotype of *Tet2*$^{-/-}$ bone marrow transplanted mice fed CDAHFD.

Lethally irradiated C57BL/6J mice were transplanted with *Tet2*$^{-/-}$ (n = 30) or control *vavCre*$^{+}$ (WT; n = 25) bone marrow cells. After hematopoietic reconstitution, mice were fed CDAHFD and body weight **(a)** and food intake **(b)** were measured over 30 days. Mice were sacrificed and terminal liver weight **(c-d)** and serum biomarkers **(e)** were measured. Control mice were transplanted with *Tet2*$^{-/-}$ (n = 6) or control *vavCre*$^{+}$ (WT; n = 6) bone marrow cells and fed standard chow for the same duration. Data from one (a-d) or two independent experiments (e) are shown. AST, aspartate transaminase; ALT, alanine transaminase; TBILI, total bilirubin; ALB, albumin; TRIG, triglycerides; GLUC, glucose; CHOL, total cholesterol; HDL, high-density lipoprotein; LDL, low-density lipoprotein; NEFA, non-essential fatty acids.

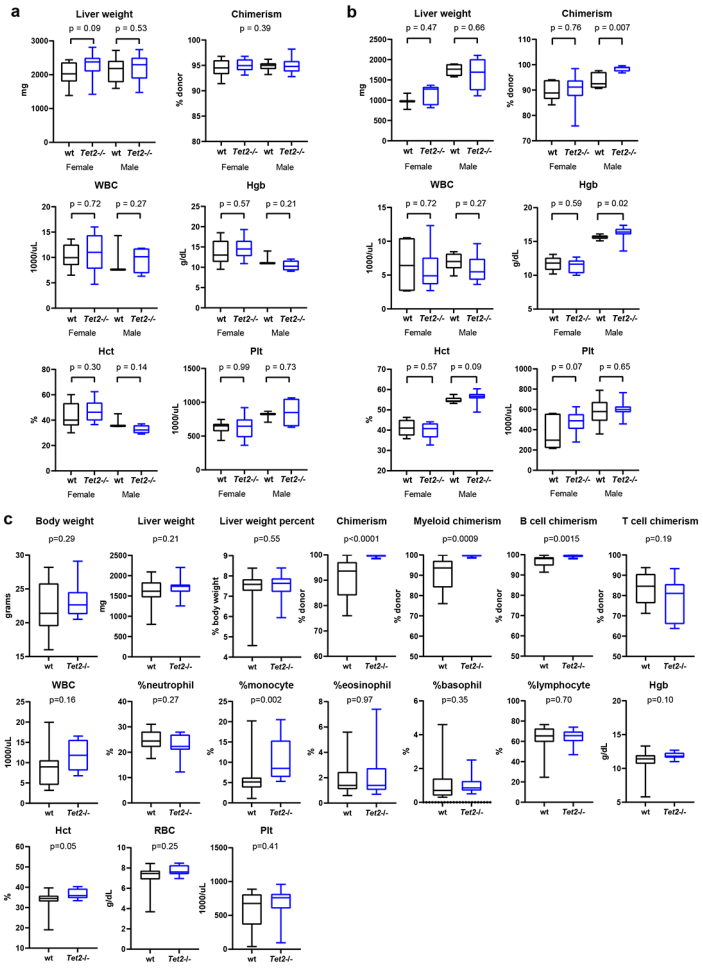

Extended Data Fig. 6. Liver and hematological parameters of *Tet2*$^{-/-}$ bone marrow transplanted mice.

a, *Ldlr*$^{-/-}$ mice were transplanted with *Tet2*$^{-/-}$ (n = 25) or control *vavCre*$^{+}$ (WT; n = 20) bone marrow cells and fed Western diet for 10 weeks. **b,** B6.SJL mice were transplanted with *Tet2*$^{-/-}$ (n = 19) or control *vavCre*$^{+}$ (WT; n = 12) bone marrow cells and fed CDAHFD for 11 weeks. **c,** C57BL/6J mice were transplanted with *Tet2*$^{-/-}$ (n = 12) or control *vavCre*$^{+}$ (WT; n = 13) bone marrow cells and fed CDAHFD for 19 weeks. After the prescribed dietary periods, mice were sacrificed and terminal liver weight and peripheral blood chimerism and hematological parameters were measured. Data from one (c) or two independent experiments (a, b) are shown. WBC, white blood cell count; Hgb, hemoglobin; Hct, hematocrit; RBC, red blood cell count; Plt, platelet count.

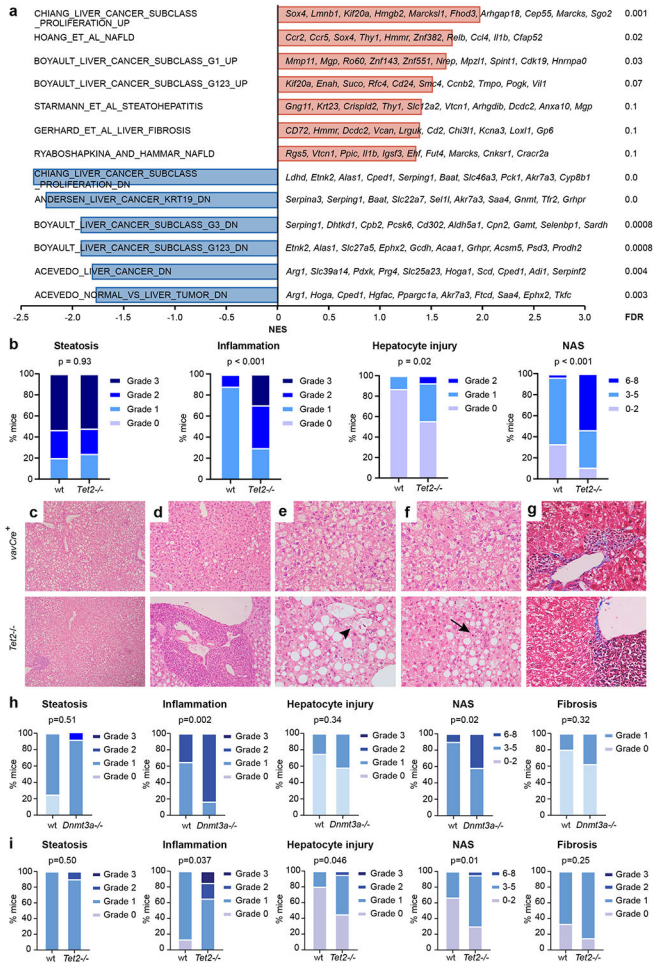

Extended Data Fig. 7. Steatohepatitis and liver fibrosis in *Tet2*$^{-/-}$ and *Dnmt3a*$^{-/-}$ transplanted mice.

a, Selected gene signatures enriched in bulk liver transcripts from *Tet2*$^{-/-}$ ($n = 4$) transplanted mice fed CDAHFD relative to control *vavCre*$^{+}$ (WT; $n = 4$) transplanted mice. **b,** Histologic features of steatohepatitis in *Ldlr*$^{-/-}$ mice transplanted with *Tet2*$^{-/-}$ ($n = 27$) and control *vavCre*$^{+}$ (WT; $n = 30$) bone marrow and fed Western diet for 10 weeks were graded on a semiquantitative scale and aggregated into a NASH activity score (NAS) using CRN histologic scoring criteria. **c-f,** Graded histologic features included steatosis (c), inflammatory foci (d), hepatocyte ballooning (e, arrowhead) and apoptosis (f, arrow). **g,** Masson's trichrome staining demonstrates absence of perivenular fibrosis in control and *Tet2*$^{-/-}$ transplanted mice. **h,** B6.SJL mice were transplanted with *Dnmt3a*$^{-/-}$ ($n = 24$) or control *vavCre*$^{+}$ (WT; $n = 20$) bone marrow cells and fed CDAHFD for 11 weeks. Steatohepatitis was assessed histologically for steatosis, inflammation, and hepatocyte ballooning. Collagen fibrosis was measured by Masson's trichrome staining. **i,** B6.SJL mice were transplanted with *Tet2*$^{-/-}$ ($n = 20$) or control *vavCre*$^{+}$ (WT; $n = 15$) bone marrow cells and fed CDAHFD for 11 weeks, then reverted to standard chow for 10 days. Compared to control animals, *Tet2*$^{-/-}$ transplanted mice show similar resolution of liver fat but show persistently greater inflammation and more hepatocyte ballooning. Collagen fibrosis, as measured by Masson's trichrome staining, was not significantly different. Data from one

(a) or two independent experiments (b, h, i) are shown. NES, normalized enrichment score; FDR, false discovery rate.

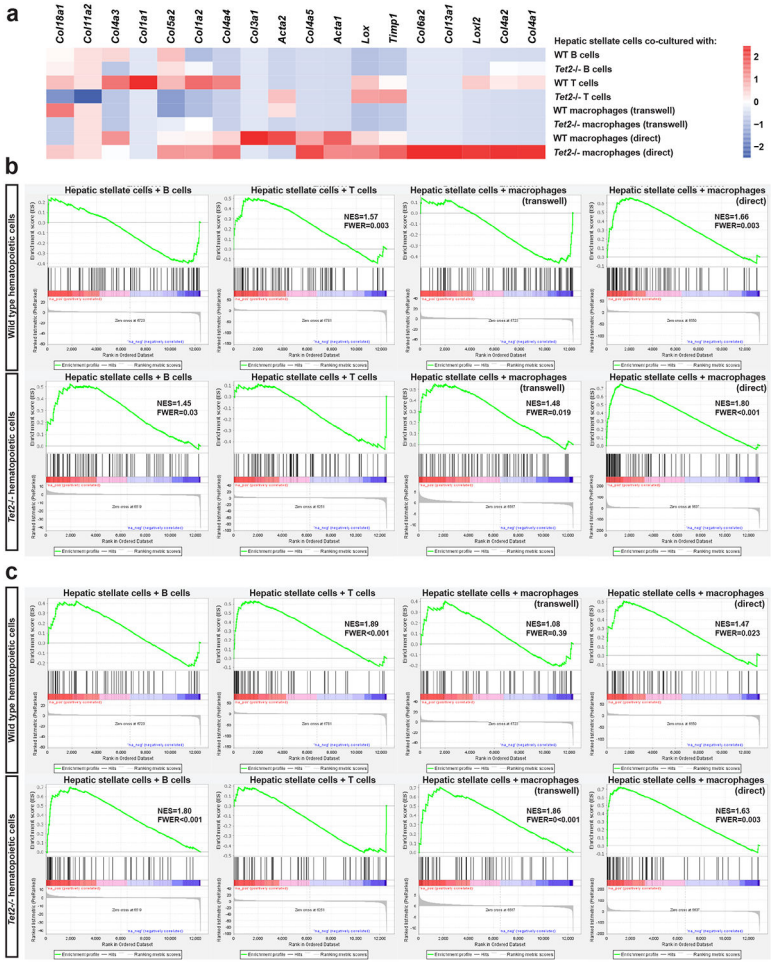

Extended Data Fig. 8. Fibrogenic response in hepatic stellate cells co-cultured with *Tet2*$^{-/-}$ hematopoietic cell populations.

Hepatic stellate cells were isolated from wild type livers (n = 5) and co-cultured with CD19^{+} B cells, CD3^{+} T cells, or CD11b^{+} hepatic macrophages isolated from *Tet2*$^{-/-}$ (n = 5) or control *vavCre*$^{+}$ (WT; n = 5) mice for 2 days. Co-cultured hepatic stellate cells were harvested for RNA sequencing and selected differentially expressed genes (relative to hepatic stellate cell mono-culture) are shown **(a)**. Gene expression profiles of co-cultured hepatic stellate cells were compared to published gene signatures of activated hepatic stellate cells from Zhang DY et al.[48] (**b**) and Wang H et al.[49] (**c**). Data from one experiment are shown. NES, normalized enrichment score; FWER, family-wise error rate.

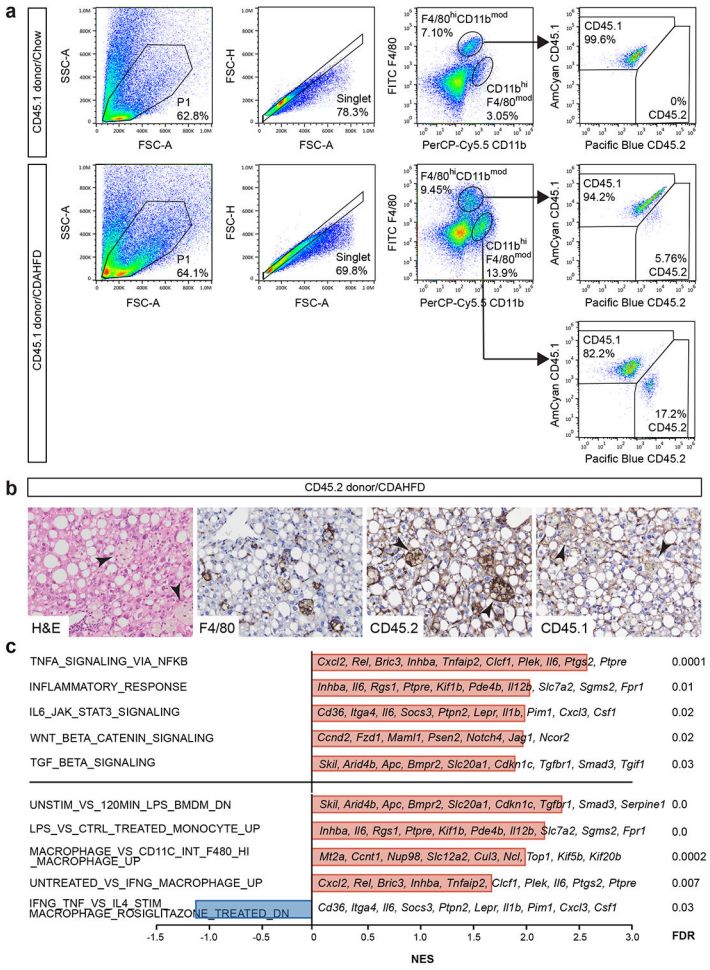

Extended Data Fig. 9. Donor-derived Kupffer cells and hepatic macrophages after bone marrow transplantation.

a, C57BL/6J mice were transplanted with CD45.1^{+} *Tet2*$^{-/-}$ (n = 2) bone marrow cells and fed CDAHFD or standard chow. After 4 weeks, mice were sacrificed and dissociated liver cells were subjected to flow cytometric analysis of CD45.1 (donor) and CD45.2 (recipient) expression in F4/80^{hi}CD11b^{mod} Kupffer cells and CD11b^{hi}F4/80^{mod} hepatic macrophages. **b,** B6.SJL mice were transplanted with CD45.2^{+} *vavCre*$^{+}$ (n = 2) bone marrow cells and fed CDAHFD or standard chow for 19 weeks. Immunohistochemical stains demonstrate the presence of CD45.2^{+}CD45.1^{-}F4/80^{+} macrophages (arrowheads) in livers of bone marrow transplanted mice fed CDAHFD. Representative data from one mouse per condition are shown. **c,** Selected gene signatures enriched in sorted liver macrophages from *Tet2*$^{-/-}$ (n = 4) transplanted mice fed CDAHFD relative to control *vavCre*$^{+}$ (WT; n = 4) transplanted mice. Data shown are from one experiment. NES, normalized enrichment score; FWER, family-wise error rate.

Supplementary Material

Refer to Web version on PubMed Central for supplementary material.

Acknowledgements

The UK Biobank analyses were carried out under application numbers 7089 and 50834. The investigators thank the UK Biobank staff and participants. P.N. is supported by a Hassenfeld Scholar Award and the Paul & Phyllis Fireman Endowed Chair in Vascular Medicine from the Massachusetts General Hospital, and grants from the National Heart, Lung, and Blood Institute (R01HL142711, R01HL148565 and R01HL148050) and the National Institute of Diabetes and Digestive and Kidney Diseases (R01DK125782). P.N. and B.L.E. are supported by a grant from the Fondation Leducq (TNE-18CVD04). B.L.E. is also supported by the NIH (R01HL082945, P01CA108631 and P50CA206963) and the Howard Hughes Medical Institute. W.J.W. is supported by a RUNX1 Research Program and Alex's Lemonade Stand Foundation Early Career Investigator Grant. S.M.Z. was supported by the NIH National Heart, Lung, and Blood Institute (1F30HL149180-01) and the NIH Medical Scientist Training Program Training Grant (T32GM136651). A.N. was supported by funds from the Knut and Alice Wallenberg Foundation (KAW2017.0436). J.P.P. is supported by the NIH (K08HL159346). L.D. was supported by NIH grant K23 DK113220. C.J.G. is supported by the NIH (K08CA263555). R.S.S. is supported by a Kay Kendall Leukaemia Fund Intermediate Fellowship and by a CRUK Advanced Clinician Scientist Fellowship. A.V. received the Harold M. English Fellowship Fund from Harvard Medical School (Boston, USA). P.G.K. is supported by the Damon Runyon Physician-Scientist Award (PST-35-21) and the Edward P. Evans Foundation Evans Young Investigator Award. M.A. was supported by the Deutsche Forschungsgemeinschaft (DFG, AG252/1-1). P.-R.L. is supported by NIH grant DP2 ES030554 and a Burroughs Wellcome Fund Career Award at the Scientific Interfaces. R.T.C. is supported by NIH grants R01AI136715 and R01AI155140, and the MGH Research Scholars Program. Molecular data for the Trans-Omics in Precision Medicine (TOPMed) programme were supported by the National Heart, Lung, and Blood Institute. See Supplementary Table 14 for TOPMed-specific omics support information. Core support including centralized genomic read mapping and genotype calling, along with variant quality metrics and filtering, was provided by the TOPMed Informatics Research Center (3R01HL-117626-02S1; contract HHSN268201800002I). Core support including phenotype harmonization, data management, sample-identity quality control and general programme coordination were provided by the TOPMed Data Coordinating Center (R01HL-120393; U01HL-120393; contract HHSN268201800001I). We gratefully acknowledge the studies and participants who provided biological samples and data for TOPMed. We thank D. K. Li and P. G. Miller for experimental advice and critical reading of the manuscript. The views expressed in this manuscript are those of the authors and do not necessarily represent the views of the National Heart, Lung, and Blood Institute; the National Institutes of Health; or the US Department of Health and Human Services.

Data Availability

Source data used in this analysis are available to approved researchers through ARIC, TOPMed, the UK Biobank and MGB Biobank. CHIP variants identified in this study are listed in Supplementary Tables 3 and 12. Full summary statistics for the cirrhosis GWAS are available for download at https://cvd.hugeamp.org/downloads.html. RNA-sequencing datasets are available in the Gene Expression Omnibus repository under the accession code GSE223695.

NHLBI TOPMed Hematology Working Group

Namiko Abe[32], Gonçalo Abecasis[33], Francois Aguet[34], Christine Albert[35], Laura Almasy[36], Alvaro Alonso[37], Seth Ament[38], Peter Anderson[39], Pramod Anugu[40], Deborah Applebaum-Bowden[41], Kristin Ardlie[34], Dan Arking[42], Donna K Arnett[43], Allison Ashley-Koch[44], Stella Aslibekyan[45], Tim Assimes[46], Paul Auer[47], Dimitrios Avramopoulos[42], Najib Ayas[48], Adithya Balasubramanian[49], John Barnard[50], Kathleen Barnes[51], R. Graham Barr[52], Emily Barron-Casella[42], Lucas Barwick[53], Terri Beaty[42], Gerald Beck[50], Diane Becker[42], Lewis Becker[42], Rebecca Beer[54], Amber Beitelshees[38], Emelia Benjamin[55], Takis Benos[56], Marcos Bezerra[57], Larry Bielak[33], Joshua Bis[39], Thomas Blackwell[33], John Blangero[58], Nathan Blue[59], Donald W. Bowden[60], Russell Bowler[61], Jennifer Brody[39], Ulrich Broeckel[47], Jai Broome[39], Deborah Brown[62], Karen Bunting[32], Esteban Burchard[63], Carlos Bustamante[46], Erin Buth[39], Brian Cade[64], Jonathan Cardwell[65], Vincent Carey[64], Julie Carrier[66], April P. Carson[40], Cara Carty[67], Richard Casaburi[68], Juan P

Casas Romero[64], James Casella[42], Peter Castaldi[64], Mark Chaffin[34], Christy Chang[38], Yi-Cheng Chang[69], Daniel Chasman[64], Sameer Chavan[65], Bo-Juen Chen[32], Wei-Min Chen[70], Yii-Der Ida Chen[71], Michael Cho[64], Seung Hoan Choi[34], Lee-Ming Chuang[69], Mina Chung[50], Ren-Hua Chung[72], Clary Clish[34], Suzy Comhair[50], Matthew Conomos[39], Elaine Cornell[73], Adolfo Correa[40], Carolyn Crandall[68], James Crapo[61], L. Adrienne Cupples[74], Joanne Curran[58], Jeffrey Curtis[33], Brian Custer[75], Coleen Damcott[38], Dawood Darbar[76], Sean David[77], Colleen Davis[39], Michelle Daya[65], Mariza de Andrade[78], Lisa de las Fuentes[79], Paul de Vries[62], Michael DeBaun[80], Ranjan Deka[81], Dawn DeMeo[64], Scott Devine[38], Huyen Dinh[49], Harsha Doddapaneni[49], Qing Duan[82], Shannon Dugan-Perez[49], Ravi Duggirala[58], Jon Peter Durda[73], Susan K. Dutcher[79], Charles Eaton[83], Lynette Ekunwe[40], Adel El Boueiz[84], Patrick Ellinor[85], Leslie Emery[39], Serpil Erzurum[50], Charles Farber[70], Jesse Farek[49], Tasha Fingerlin[61], Matthew Flickinger[33], Myriam Fornage[62], Nora Franceschini[82], Chris Frazar[39], Mao Fu[38], Stephanie M. Fullerton[39], Lucinda Fulton[79], Stacey Gabriel[34], Weiniu Gan[54], Shanshan Gao[65], Yan Gao[40], Margery Gass[86], Heather Geiger[32], Bruce Gelb[87], Mark Geraci[88], Soren Germer[32], Robert Gerszten[89], Auyon Ghosh[64], Richard Gibbs[49], Chris Gignoux[46], Mark Gladwin[88], David Glahn[90], Stephanie Gogarten[39], Da-Wei Gong[38], Harald Goring[58], Sharon Graw[91], Kathryn J. Gray[92], Daniel Grine[65], Colin Gross[33], C. Charles Gu[79], Yue Guan[38], Xiuqing Guo[71], Namrata Gupta[34], Jeff Haessler[86], Michael Hall[40], Yi Han[49], Patrick Hanly[93], Daniel Harris[38], Nicola L. Hawley[94], Jiang He[95], Ben Heavner[39], Susan Heckbert[39], Ryan Hernandez[63], David Herrington[60], Craig Hersh[64], Bertha Hidalgo[45], James Hixson[62], Brian Hobbs[64], John Hokanson[65], Elliott Hong[38], Karin Hoth[96], Chao (Agnes) Hsiung[72], Jianhong Hu[49], Yi-Jen Hung[97], Haley Huston[98], Chii Min Hwu[99], Marguerite Ryan Irvin[45], Rebecca Jackson[100], Deepti Jain[39], Cashell Jaquish[54], Jill Johnsen[39], Craig Johnson[39], Rich Johnston[37], Kimberly Jones[42], Hyun Min Kang[33], Robert Kaplan[101], Sharon Kardia[33], Shannon Kelly[63], Eimear Kenny[87], Michael Kessler[38], Alyna Khan[39], Ziad Khan[49], Wonji Kim[84], John Kimoff[102], Greg Kinney[65], Barbara Konkle[98], Charles Kooperberg[86], Holly Kramer[103], Christoph Lange[104], Ethan Lange[65], Leslie Lange[65], Cathy Laurie[39], Cecelia Laurie[39], Meryl LeBoff[64], Jiwon Lee[64], Sandra Lee[49], Wen-Jane Lee[99], Jonathon LeFaive[33], David Levine[39], Joshua Lewis[38], Xiaohui Li[71], Yun Li[82], Henry Lin[71], Honghuang Lin[74], Xihong Lin[104], Simin Liu[83], Yongmei Liu[44], Yu Liu[46], Ruth J.F. Loos[87], Steven Lubitz[85], Kathryn Lunetta[74], James Luo[54], Ulysses Magalang[105], Michael Mahaney[58], Barry Make[42], Ani Manichaikul[70], Alisa Manning[106], JoAnn Manson[64], Lisa Martin[107], Melissa Marton[32], Susan Mathai[65], Rasika Mathias[42], Susanne May[39], Patrick McArdle[38], Merry-Lynn McDonald[45], Sean McFarland[84], Stephen McGarvey[83], Daniel McGoldrick[39], Caitlin McHugh[39], Becky McNeil[108], Hao Mei[40], James Meigs[85], Vipin Menon[49], Luisa Mestroni[91], Ginger Metcalf[49], Deborah A Meyers[109], Emmanuel Mignot[46], Julie Mikulla[54], Nancy Min[40], Mollie Minear[110], Ryan L Minster[88], Braxton D. Mitchell[38], Matt Moll[64], Zeineen Momin[49], May E. Montasser[38], Courtney Montgomery[111], Donna Muzny[49], Josyf C Mychaleckyj[70], Girish Nadkarni[87], Rakhi Naik[42], Take Naseri[112], Sergei Nekhai[113], Sarah C. Nelson[39], Bonnie Neltner[65], Caitlin Nessner[49], Deborah Nickerson[39], Osuji Nkechinyere[49], Kari North[82], Jeff O'Connell[38], Tim O'Connor[38], Heather Ochs-Balcom[114], Geoffrey Okwuonu[49], Allan Pack[115], David T. Paik[46], Nicholette Palmer[60], James Pankow[116], George Papanicolaou[54], Cora Parker[108], Gina Peloso[74], Juan Manuel Peralta[58], Marco Perez[46], James Perry[38], Ulrike Peters[86], Patricia Peyser[33], Lawrence S

Phillips[37], Jacob Pleiness[33], Toni Pollin[38], Wendy Post[42], Julia Powers Becker[65], Meher Preethi Boorgula[65], Michael Preuss[87], Bruce Psaty[39], Pankaj Qasba[54], Dandi Qiao[64], Zhaohui Qin[37], Nicholas Rafaels[65], Laura Raffield[82], Mahitha Rajendran[49], D.C. Rao[79], Laura Rasmussen-Torvik[117], Aakrosh Ratan[70], Susan Redline[64], Robert Reed[38], Catherine Reeves[32], Elizabeth Regan[61], Alex Reiner[118], Muagututi'a Sefuiva Reupena[119], Ken Rice[39], Stephen Rich[70], Rebecca Robillard[120], Nicolas Robine[32], Dan Roden[80], Carolina Roselli[34], Jerome Rotter[71], Ingo Ruczinski[42], Alexi Runnels[32], Pamela Russell[65], Sarah Ruuska[39], Kathleen Ryan[38], Ester Cerdeira Sabino[121], Danish Saleheen[52], Shabnam Salimi[38], Sejal Salvi[49], Steven Salzberg[42], Kevin Sandow[71], Vijay G. Sankaran[84], Jireh Santibanez[49], Karen Schwander[79], David Schwartz[65], Frank Sciurba[88], Christine Seidman[122], Jonathan Seidman[122], Frédéric Sériès[123], Vivien Sheehan[37], Stephanie L. Sherman[37], Amol Shetty[38], Aniket Shetty[65], Wayne Hui-Heng Sheu[99], M. Benjamin Shoemaker[80], Brian Silver[124], Edwin Silverman[64], Robert Skomro[125], Albert Vernon Smith[33], Jennifer Smith[33], Josh Smith[39], Nicholas Smith[39], Tanja Smith[32], Sylvia Smoller[101], Beverly Snively[60], Michael Snyder[46], Tamar Sofer[64], Nona Sotoodehnia[39], Adrienne M. Stilp[39], Garrett Storm[65], Elizabeth Streeten[38], Jessica Lasky Su[64], Yun Ju Sung[79], Jody Sylvia[64], Adam Szpiro[39], Daniel Taliun[33], Hua Tang[46], Margaret Taub[42], Kent D. Taylo r[71], Matthew Taylor[91], Simeon Taylor[38], Marilyn Telen[44], Timothy A. Thornton[39], Machiko Threlkeld[39], Lesley Tinker[86], David Tirschwell[39], Sarah Tishkoff[115], Hemant Tiwari[45], Catherine Tong[39], Russell Tracy[73], Michael Tsai[116], Dhananjay Vaidya[42], David Van Den Berg[126], Peter VandeHaar[33], Scott Vrieze[116], Tarik Walker[65], Robert Wallace[96], Avram Walts[65], Fei Fei Wang[39], Heming Wang[127], Jiongming Wang[33], Karol Watson[68], Jennifer Watt[49], Daniel E. Weeks[88], Bruce Weir[39], Scott T Weiss[64], Lu-Chen Weng[85], Jennifer Wessel[128], Cristen Willer[33], Kayleen Williams[39], L. Keoki Williams[129], Scott Williams[130], Carla Wilson[64], James Wilson[89], Lara Winterkorn[32], Quenna Wong[39], Joseph Wu[46], Huichun Xu[38], Lisa Yanek[42], Ivana Yang[65], Ketian Yu[33], Yingze Zhang[88], Snow Xueyan Zhao[61], Wei Zhao[33], Xiaofeng Zhu[130], Elad Ziv[63], Michael Zody[32], Sebastian Zoellner[33]

32) New York Genome Center, New York, NY, USA

33) University of Michigan, Ann Arbor, MI, USA

34) Broad Institute, Cambridge, MA, USA

35) Cedars Sinai, Los Angeles, CA, USA

36) Children's Hospital of Philadelphia, University of Pennsylvania, Philadelphia, PA, USA

37) Emory University, Atlanta, GA, USA

38) University of Maryland, College Park, MD, USA

39) University of Washington, Seattle, WA, USA

40) University of Mississippi, Oxford, MS, USA

41) National Institutes of Health, Bethesda, MD, USA

42) Johns Hopkins University, Baltimore, MD, USA

43) University of South Carolina, Columbia, SC, USA

44) Duke University, Durham, NC, USA

45) University of Alabama, Tuscaloosa, AL, USA

46) Stanford University, Stanford, CA, USA

47) Medical College of Wisconsin, Milwaukee, WI, USA

48) Providence Health Care, Vancouver, BC, Canada

49) Baylor College of Medicine Human Genome Sequencing Center, Houston, TX, USA

50) Cleveland Clinic, Cleveland, OH, USA

51) Tempus, University of Colorado Anschutz Medical Campus, Aurora, CO, USA

52) Columbia University, New York, NY, USA

53) The Emmes Corporation, Rockville, MD, USA

54) National Heart, Lung, and Blood Institute, National Institutes of Health, Bethesda, MD, USA

55) Boston University, Massachusetts General Hospital, Boston, MA, USA

56) University of Pittsburgh, Pittsburgh, PA, USA

57) Fundação de Hematologia e Hemoterapia de Pernambuco (Hemope), Recife, Brazil

58) University of Texas Rio Grande Valley School of Medicine, Edinburg, TX, USA

59) University of Utah, Salt Lake City, UT, USA

60) Wake Forest Baptist Health, Winston-Salem, NC, USA

61) National Jewish Health, Denver, CO, USA

62) University of Texas Health at Houston, Houston, TX, USA

63) University of California, San Francisco, San Francisco, CA, USA

64) Brigham & Women's Hospital, Boston, MA, USA

65) University of Colorado at Denver, Denver, CO, USA

66) University of Montreal, Montreal, QC, Canada

67) Washington State University, Pullman, WA, USA

68) University of California, Los Angeles, Los Angeles, CA, USA

69) National Taiwan University, Taipei, Taiwan

70) University of Virginia, Charlottesville, VA, USA

71) Lundquist Institute, Torrance, CA, USA

72) National Health Research Institute Taiwan, Miaoli, Taiwan

73) University of Vermont, Burlington, VT, USA

74) Boston University, Boston, MA, USA

75) Vitalant Research Institute, San Francisco, CA, USA

76) University of Illinois at Chicago, Chicago, IL, USA

77) University of Chicago, Chicago, IL, USA

78) Mayo Clinic, Rochester, MN, USA

79) Washington University in St Louis, St. Louis, MO, USA

80) Vanderbilt University, Nashville, TN, USA

81) University of Cincinnati, Cincinnati, OH, USA

82) University of North Carolina, Chapel Hill, NC, USA

83) Brown University, Providence, RI, USA

84) Harvard University, Cambridge, MA, USA

85) Massachusetts General Hospital, Boston, MA, USA

86) Fred Hutchinson Cancer Research Center, Seattle, WA, USA

87) Icahn School of Medicine at Mount Sinai, New York, NY, USA

88) University of Pittsburgh, Pittsburgh, PA, USA

89) Beth Israel Deaconess Medical Center, Boston, MA, USA

90) Boston Children's Hospital, Harvard Medical School, Boston, MA, USA

91) University of Colorado Anschutz Medical Campus, Aurora, CO, USA

92) Mass General Brigham, Boston, MA, USA

93) University of Calgary, Calgary, Alberta, Canada

94) Yale University, New Haven, CT, USA

95) Tulane University, New Orleans, LA, USA

96) University of Iowa, Iowa City, IA, USA

97) Tri-Service General Hospital National Defense Medical Center, Taipei, Taiwan

98) Blood Works Northwest, Seattle, WA, USA

99) Taichung Veterans General Hospital Taiwan, Taichung, Taiwan

100) Oklahoma State University Medical Center, Tulsa, OK, USA

101) Albert Einstein College of Medicine, Bronx, NY, USA

102) McGill University, Montreal, Quebec, Canada

103) Loyola University, Chicago, IL, USA

104) Harvard School of Public Health, Boston, MA, USA

105) The Ohio State University, Columbus, OH, USA

106) Broad Institute, Harvard University, Massachusetts General Hospital, Cambridge, MA, USA

107) George Washington University, Washington, D.C., USA

108) RTI International, Research Triangle Park, NC, USA

109) University of Arizona, Tucson, AZ, USA

110) National Institute of Child Health and Human Development, National Institutes of Health, Bethesda, MD, USA

111) Oklahoma Medical Research Foundation, Oklahoma City, OK, USA

112) Ministry of Health, Government of Samoa, Apia, Samoa

113) Howard University, Washington, D.C., USA

114) University at Buffalo, Buffalo, NY, USA

115) University of Pennsylvania, Philadelphia, PA, USA

116) University of Minnesota, Minneapolis, MN, USA

117) Northwestern University, Evanston, IL, USA

118) Fred Hutchinson Cancer Research Center, University of Washington, Seattle, WA, USA

119) Lutia i Puava Ae Mapu i Fagalele, Apia, Samoa

120) University of Ottawa, Ottawa, Ontario, Canada

121) Universidade de Sao Paulo, São Paulo, Brazil

122) Harvard Medical School, Boston, MA, USA

123) Université Laval, Quebec City, Quebec, Canada

124) UMass Memorial Medical Center, Worcester, MA, USA

125) University of Saskatchewan, Saskatoon, Saskatchewan, Canada

126) University of Southern California, Los Angeles, CA, USA

127) Brigham & Women's Hospital, Mass General Brigham, Boston, MA, USA

128) Indiana University, Bloomington, IN, USA

129) Henry Ford Health System, Detroit, MI, USA

130) Case Western Reserve University, Cleveland, OH, USA

References

1. Anstee QM, Reeves HL, Kotsiliti E, Govaere O & Heikenwalder M From NASH to HCC: current concepts and future challenges. Nat. Rev. Gastroenterol. Hepatol 16, 411–428 (2019). [PubMed: 31028350]
2. Kisseleva T & Brenner D Molecular and cellular mechanisms of liver fibrosis and its regression. Nat. Rev. Gastroenterol. Hepatol 18, 151–166 (2021). [PubMed: 33128017]
3. Younossi ZM et al. Epidemiology of chronic liver diseases in the USA in the past three decades. Gut 69, 564–568 (2020). [PubMed: 31366455]
4. Scaglione S. et al. The Epidemiology of Cirrhosis in the United States: A Population-based Study. J. Clin. Gastroenterol 49, 690–696 (2015). [PubMed: 25291348]
5. Brempelis KJ & Crispe IN Infiltrating monocytes in liver injury and repair. Clin. Transl. Immunol 5, e113 (2016).
6. Krenkel O & Tacke F Liver macrophages in tissue homeostasis and disease. Nat. Rev. Immunol 17, 306–321 (2017). [PubMed: 28317925]
7. Baeck C. et al. Pharmacological inhibition of the chemokine CCL2 (MCP-1) diminishes liver macrophage infiltration and steatohepatitis in chronic hepatic injury. Gut 61, 416–426 (2012). [PubMed: 21813474]
8. Krenkel O. et al. Therapeutic inhibition of inflammatory monocyte recruitment reduces steatohepatitis and liver fibrosis. Hepatol. Baltim. Md 67, 1270–1283 (2018).
9. Krenkel O. et al. Myeloid cells in liver and bone marrow acquire a functionally distinct inflammatory phenotype during obesity-related steatohepatitis. Gut 69, 551–563 (2020). [PubMed: 31076404]
10. Steensma DP et al. Clonal hematopoiesis of indeterminate potential and its distinction from myelodysplastic syndromes. Blood 126, 9–16 (2015). [PubMed: 25931582]
11. Jaiswal S. et al. Age-related clonal hematopoiesis associated with adverse outcomes. N. Engl. J. Med 371, 2488–2498 (2014). [PubMed: 25426837]
12. Xie M. et al. Age-related mutations associated with clonal hematopoietic expansion and malignancies. Nat. Med 20, 1472–1478 (2014). [PubMed: 25326804]

13. Genovese G. et al. Clonal hematopoiesis and blood-cancer risk inferred from blood DNA sequence. N. Engl. J. Med 371, 2477–2487 (2014). [PubMed: 25426838]
14. Jaiswal S. et al. Clonal Hematopoiesis and Risk of Atherosclerotic Cardiovascular Disease. N. Engl. J. Med 377, 111–121 (2017). [PubMed: 28636844]
15. Bick AG et al. Genetic Interleukin 6 Signaling Deficiency Attenuates Cardiovascular Risk in Clonal Hematopoiesis. Circulation 141, 124–131 (2020). [PubMed: 31707836]
16. Fuster JJ et al. Clonal hematopoiesis associated with TET2 deficiency accelerates atherosclerosis development in mice. Science 355, 842–847 (2017). [PubMed: 28104796]
17. Sano S et al. Tet2-Mediated Clonal Hematopoiesis Accelerates Heart Failure Through a Mechanism Involving the IL-1β/NLRP3 Inflammasome. J. Am. Coll. Cardiol 71, 875–886 (2018). [PubMed: 29471939]
18. Loh P-R et al. Insights about clonal hematopoiesis from 8,342 mosaic chromosomal alterations. Nature 559, 350–355 (2018). [PubMed: 29995854]
19. Bick AG et al. Inherited causes of clonal haematopoiesis in 97,691 whole genomes. Nature 586, 763–768 (2020). [PubMed: 33057201]
20. Emdin CA et al. A missense variant in Mitochondrial Amidoxime Reducing Component 1 gene and protection against liver disease. PLoS Genet. 16, e1008629 (2020). [PubMed: 32282858]
21. Bao EL et al. Inherited myeloproliferative neoplasm risk affects haematopoietic stem cells. Nature 586, 769–775 (2020). [PubMed: 33057200]
22. Matsumoto M et al. An improved mouse model that rapidly develops fibrosis in non-alcoholic steatohepatitis. Int. J. Exp. Pathol 94, 93–103 (2013). [PubMed: 23305254]
23. Ikawa-Yoshida A et al. Hepatocellular carcinoma in a mouse model fed a choline-deficient, L-amino acid-defined, high-fat diet. Int. J. Exp. Pathol 98, 221–233 (2017). [PubMed: 28895242]
24. Buzzetti E, Pinzani M & Tsochatzis EA The multiple-hit pathogenesis of non-alcoholic fatty liver disease (NAFLD). Metabolism. 65, 1038–1048 (2016). [PubMed: 26823198]
25. Klein I. et al. Kupffer cell heterogeneity: functional properties of bone marrow derived and sessile hepatic macrophages. Blood 110, 4077–4085 (2007). [PubMed: 17690256]
26. Scott CL et al. Bone marrow-derived monocytes give rise to self-renewing and fully differentiated Kupffer cells. Nat. Commun 7, 10321 (2016). [PubMed: 26813785]
27. Oo YH et al. Distinct Roles for CCR4 and CXCR3 in the Recruitment and Positioning of Regulatory T Cells in the Inflamed Human Liver. J. Immunol 184, 2886–2898 (2010). [PubMed: 20164417]
28. Fuster JJ et al. TET2-Loss-of-Function-Driven Clonal Hematopoiesis Exacerbates Experimental Insulin Resistance in Aging and Obesity. Cell Rep. 33, 108326 (2020). [PubMed: 33113366]
29. Zhao Q, Wang J, Hemani G, Bowden J & Small DS Statistical inference in two-sample summary-data Mendelian randomization using robust adjusted profile score. Ann. Stat 48, 1742–1769 (2020).
30. Wunderlich FT et al. Interleukin-6 signaling in liver-parenchymal cells suppresses hepatic inflammation and improves systemic insulin action. Cell Metab. 12, 237–249 (2010). [PubMed: 20816090]
31. Yamaguchi K. et al. Blockade of interleukin-6 signaling enhances hepatic steatosis but improves liver injury in methionine choline-deficient diet-fed mice. Lab. Investig. J. Tech. Methods Pathol 90, 1169–1178 (2010).
32. Mridha AR et al. NLRP3 inflammasome blockade reduces liver inflammation and fibrosis in experimental NASH in mice. J. Hepatol 66, 1037–1046 (2017). [PubMed: 28167322]
33. Wree A et al. NLRP3 inflammasome activation results in hepatocyte pyroptosis, liver inflammation, and fibrosis in mice. Hepatol. Baltim. Md 59, 898–910 (2014).
34. Csak T. et al. Fatty acid and endotoxin activate inflammasomes in mouse hepatocytes that release danger signals to stimulate immune cells. Hepatol. Baltim. Md 54, 133–144 (2011).

Methods references

35. Chalasani N. et al. The diagnosis and management of nonalcoholic fatty liver disease: Practice guidance from the American Association for the Study of Liver Diseases. Hepatology 67, 328–357 (2018). [PubMed: 28714183]
36. Banerjee R. et al. Multiparametric magnetic resonance for the non-invasive diagnosis of liver disease. J. Hepatol 60, 69–77 (2014). [PubMed: 24036007]
37. Kleiner DE et al. Design and validation of a histological scoring system for nonalcoholic fatty liver disease. Hepatology 41, 1313–1321 (2005). [PubMed: 15915461]
38. Duewell P. et al. NLRP3 inflamasomes are required for atherogenesis and activated by cholesterol crystals that form early in disease. Nature 464, 1357–1361 (2010). [PubMed: 20428172]
39. Hoang SA et al. Gene Expression Predicts Histological Severity and Reveals Distinct Molecular Profiles of Nonalcoholic Fatty Liver Disease. Sci. Rep 9, 12541 (2019). [PubMed: 31467298]
40. Ryaboshapkina M & Hammar M Human hepatic gene expression signature of non-alcoholic fatty liver disease progression, a meta-analysis. Sci. Rep 7, (2017).
41. Gerhard GS et al. Transcriptomic Profiling of Obesity-Related Nonalcoholic Steatohepatitis Reveals a Core Set of Fibrosis-Specific Genes. J. Endocr. Soc 2, 710–726 (2018). [PubMed: 29978150]
42. Verbanck M, Chen C-Y, Neale B & Do R Detection of widespread horizontal pleiotropy in causal relationships inferred from Mendelian randomization between complex traits and diseases. Nat. Genet 50, 693–698 (2018). [PubMed: 29686387]
43. Burgess S & Thompson SG Interpreting findings from Mendelian randomization using the MR-Egger method. Eur. J. Epidemiol 32, 377–389 (2017). [PubMed: 28527048]
44. Liu M. et al. Association studies of up to 1.2 million individuals yield new insights into the genetic etiology of tobacco and alcohol use. Nat. Genet 51, 237–244 (2019). [PubMed: 30643251]
45. Yengo L. et al. Meta-analysis of genome-wide association studies for height and body mass index in ~700000 individuals of European ancestry. Hum. Mol. Genet 27, 3641–3649 (2018). [PubMed: 30124842]
46. Mahajan A. et al. Fine-mapping type 2 diabetes loci to single-variant resolution using high-density imputation and islet-specific epigenome maps. Nat. Genet 50, 1505–1513 (2018). [PubMed: 30297969]
47. Evangelou E. et al. Genetic analysis of over 1 million people identifies 535 new loci associated with blood pressure traits. Nat. Genet 50, 1412–1425 (2018). [PubMed: 30224653]
48. Chen J. et al. The trans-ancestral genomic architecture of glycemic traits. Nat. Genet 53, 840–860 (2021). [PubMed: 34059833]
49. Pulit SL et al. Meta-analysis of genome-wide association studies for body fat distribution in 694 649 individuals of European ancestry. Hum. Mol. Genet 28, 166–174 (2019). [PubMed: 30239722]

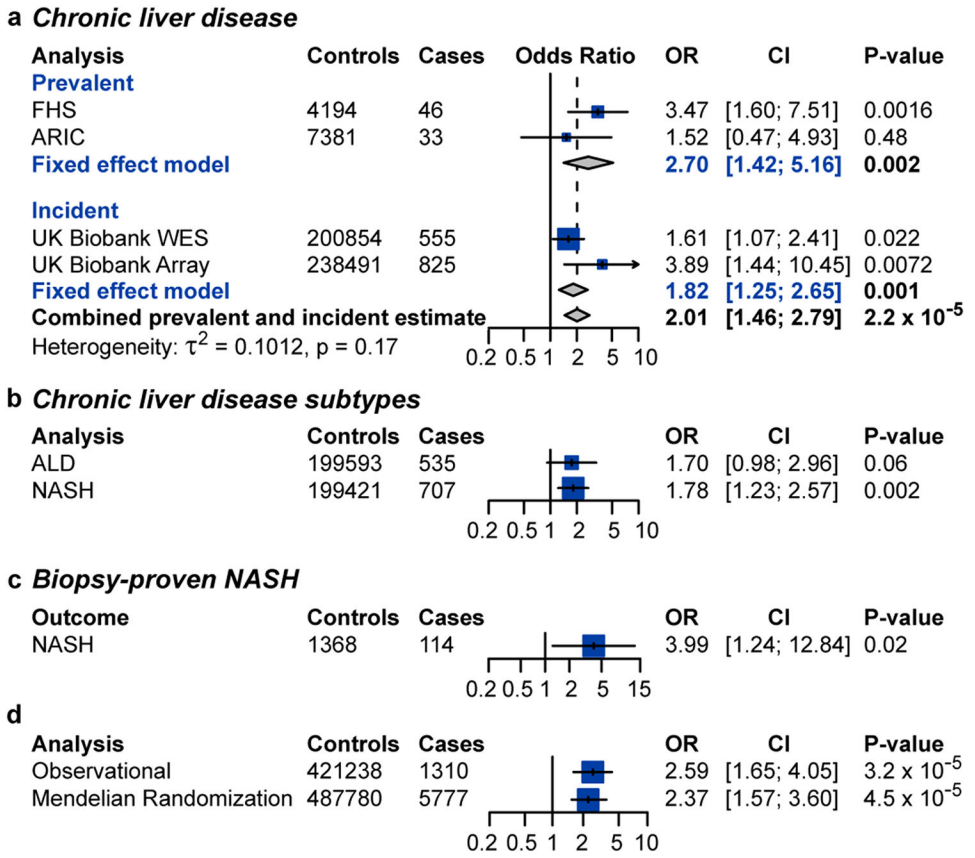

Figure 1. CHIP is associated with chronic liver disease.

a, Association of CHIP with prevalent and incident chronic liver disease. WES, whole-exome sequencing. **b**, Association of clonal haematopoiesis with subtypes of incident chronic liver disease in the UK Biobank. ALD, alcohol-related liver disease. **c**, Association of clonal haematopoiesis with biopsy-proven NASH in MGB Biobank. Estimates in prevalent analyses were derived using logistic regression, with adjustment for age, sex, type 2 diabetes and smoking. **d**, Mendelian randomization estimates of the association of CHIP with chronic liver disease. Estimates were derived using MR-RAPS with 184 independent genetic variants with significance of $P < 0.0001$. Estimates in incident analyses were derived using Cox proportional hazards regression, with adjustment for age, sex, type 2 diabetes and smoking. MGB Biobank cohorts were matched for age, sex, type 2 diabetes, body mass index and smoking. NASH was defined as chronic liver disease among individuals with a body mass index of 30 kg m^{-2} or more who consumed 21 drinks or fewer per week for men and 14 drinks or fewer per week for women. Alcohol-related liver disease was defined as chronic liver disease among individuals who consumed 21 drinks or more per week for men or 14 drinks or more per week for women.

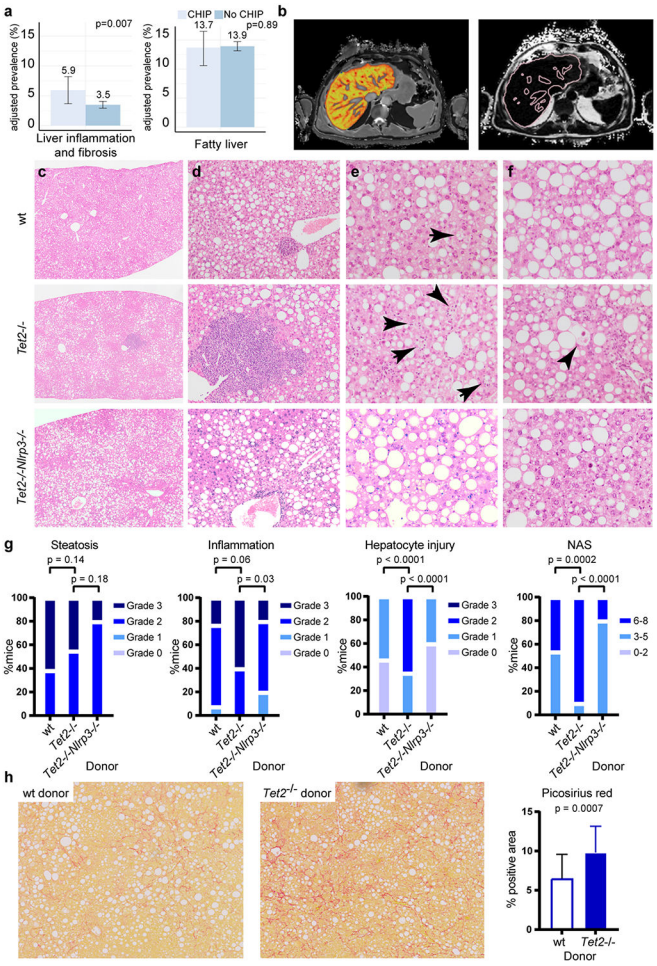

Figure 2. CHIP is associated with steatohepatitis.

a, Prevalence of liver inflammation and hepatic steatosis on magnetic resonance imaging among 8,251 individuals in the UK Biobank. Liver inflammation and fibrosis was defined as a cT1 signal ≥ 795 ms. Fatty liver was defined as a proton density fat fraction ≥ 5%. Logistic regression, with adjustment for age and sex, was used to test the association between CHIP status and the presence of fatty liver and liver inflammation. **b**, Perspectum MultiScan cT1 image (left) and proton density fat fraction (right) of a patient with CHIP. Image reproduced with permission from the UK Biobank. **c–g**, B6.SJL mice were transplanted with *Tet2*$^{-/-}$ (n = 20), *Tet2*$^{-/-}$*Nlrp3*$^{-/-}$ (n = 10) or control *vavCre*$^{+}$ (wild type (WT); n = 13) bone marrow cells and fed CDAHFD for 11 weeks. Steatohepatitis was graded using modified NASH CRN (Clinical Research Network) histologic criteria. Compared to *vavCre*$^{+}$ and *Tet2*$^{-/-}$*Nlrp3*$^{-/-}$ animals, *Tet2*$^{-/-}$-transplanted mice show similar accumulation of liver fat (**c**), increased inflammation (**d**), macrophage crown structures (**e**, arrows) and hepatocyte ballooning (**f**, arrowhead), resulting in a higher aggregate NAS (**g**). **h**, B6.SJL mice were transplanted with *Tet2*$^{-/-}$ (n = 24) or *vavCre*$^{+}$ wild-type control (n = 21) bone marrow cells and fed CDAHFD for 19 weeks. Collagen fibrosis, highlighted by Picrosirius red staining (left and middle panels), was quantified as the percentage of positive area using

ImageJ (right panel). Statistical analysis was performed using two-tailed unpaired *t*-test (**a**), chi-square test (**g**) and Mann–Whitney test (**h**). For **a** and **h**, error bars represent mean ± s.d.

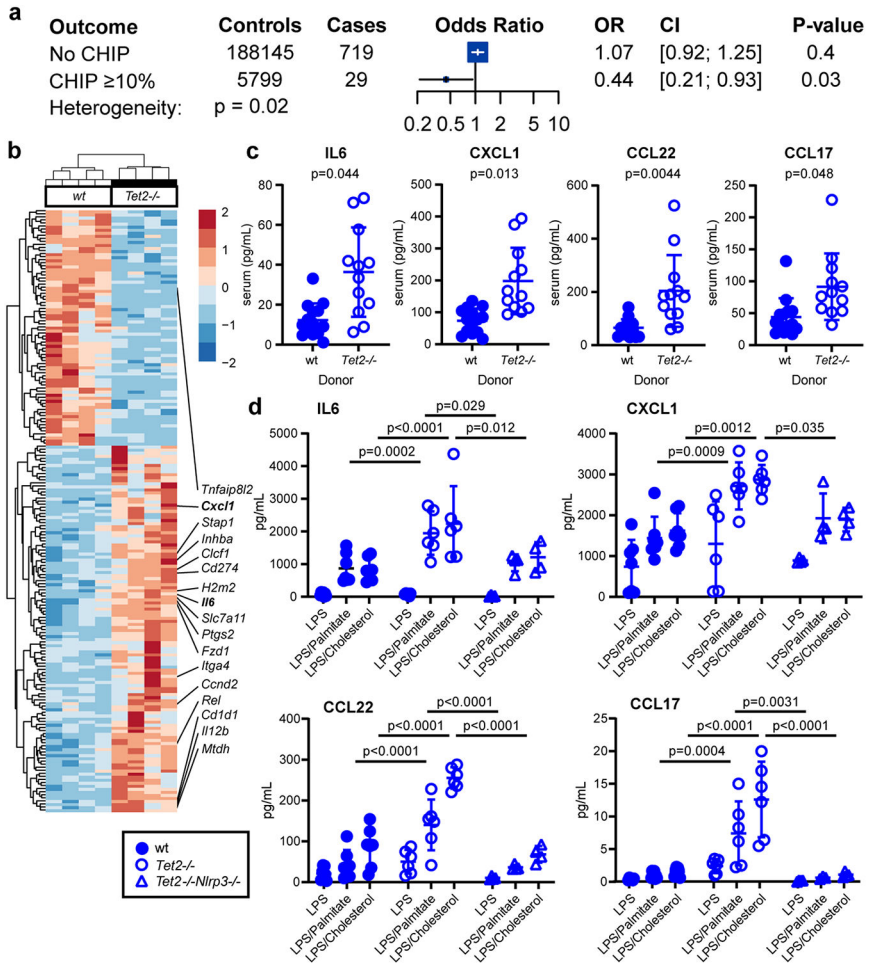

Figure 3. Proinflammatory signaling in CHIP.

a, Association of the *IL6R* germline mutation resulting in p.Asp358Ala with chronic liver disease in individuals with CHIP (variant allele fraction ≥ 10%) versus individuals without CHIP. **b**, Unsupervised hierarchical clustering of differentially regulated genes in sorted liver macrophages from B6.SJL mice transplanted with *Tet2*$^{-/-}$ (n = 4) or control *vavCre*$^{+}$ (WT; n = 4) bone marrow cells and fed CDAHFD for 11 weeks. **c**, After 19 weeks of CDAHFD, *Tet2*$^{-/-}$-transplanted (n = 12) or control *vavCre*$^{+}$-transplanted (WT; n = 14) mice were bled and serum was obtained for cytokine measurements. Statistical analysis was performed using two-tailed unpaired t-test (IL-6, CXCL1) or Mann–Whitney test (CCL22, CCL17) with Bonferroni correction for multiple hypothesis testing. **d**, Bone marrow-derived macrophages from *Tet2*$^{-/-}$ (n = 6), *Tet2*$^{-/-}$*Nlrp3*$^{-/-}$ (n = 4) or control *vavCre*$^{+}$ (WT, n = 7) mice were primed with low-dose lipopolysaccharide (LPS) for 2 h and stimulated with palmitic acid or cholesterol monohydrate crystals as indicated for 6 h. Statistical analysis was performed using two-way ANOVA. For **c** and **d**, individual measurements, mean and standard deviation from two independent experiments are shown.

Table 1.
Baseline characteristics of participants in samples analysed.

Summary of cohort characteristics in studies used for analysis of CHIP and chronic liver disease. ARIC, Atherosclerosis Risk in Communities study; BMI, body-mass index; FHS, Framingham Heart Study; MGB, Mass General Brigham; *n*, number; s.d., standard deviation; WES, whole exome sequencing; NA, not available.

Characteristics	**FHS, *n* = 4,230**	**ARIC, *n* = 7,414**	**UK Biobank WES, *n* = 201,409**	**UK Biobank Array, *n* = 239,316**	**MGB Biobank, *n* = 1,482**
Age (mean years (s.d.))	61.1 (15.7)	57.4 (6.0)	56.5 (8.1)	57.0 (8.1)	53 (12)
Women (*n* (%))	2,292 (54%)	4,358 (56%)	110,192 (55%)	127,600 (53%)	871 (59%)
BMI (mean kg/m^2 (s.d.))	27.8 (5.5)	27.7 (5.4)	27.4 (4.8)	27.4 (4.8)	NA
Current smoking (*n* (%))	610 (15%)	1,992 (26%)	13,358 (7%)	20,819 (9%)	NA
Alcohol intake (mean drinks per week (s.d.))	6.8 (16.6)	5.6 (8.8)	7.9 (9.8)	8.1 (10.3)	4.4 (7.4)
History of diabetes mellitus (*n* (%))	166 (4%)	674 (9%)	9,676 (5%)	12,438 (5%)	95 (7%)
CHIP prevalence (*n* (%))	369 (9%)	333 (4%)	11,783 (5%)	189 (0.1%)	90 (6%)
$CHIP_{\geq 10\%}$ prevalence (*n* (%))	342 (8%)	267 (4%)	6,188 (3%)	189 (0.1%)	51 (4%)